
LEARNABLE GRAPH CONVOLUTIONAL ATTENTION NETWORKS

Adrián Javaloy^{1*} Pablo Sánchez-Martín^{1,2*} Amit Levi³ Isabel Valera^{1,4}

¹Department of Computer Science of Saarland University, Saarbrücken, Germany

²Max Planck Institute for Intelligent Systems, Tübingen, Germany

³Huawei Noah's Ark Lab, Montreal, Canada

⁴Max Planck Institute for Software Systems, Saarbrücken, Germany

ABSTRACT

Existing Graph Neural Networks (GNNs) compute the message exchange between nodes by either aggregating uniformly (*convolving*) the features of all the neighboring nodes, or by applying a non-uniform score (*attending*) to the features. Recent works have shown the strengths and weaknesses of the resulting GNN architectures, respectively, GCNs and GATs. In this work, we aim at exploiting the strengths of both approaches to their full extent. To this end, we first introduce the graph convolutional attention layer (CAT), which relies on convolutions to compute the attention scores. Unfortunately, as in the case of GCNs and GATs, we show that there exists no clear winner between the three—neither theoretically nor in practice—as their performance directly depends on the nature of the data (i.e., of the graph and features). This result brings us to the main contribution of our work, the learnable graph convolutional attention network (L-CAT): a GNN architecture that automatically interpolates between GCN, GAT and CAT in each layer, by adding two scalar parameters. Our results demonstrate that L-CAT is able to efficiently combine different GNN layers along the network, outperforming competing methods in a wide range of datasets, and resulting in a more robust model that reduces the need of cross-validating.

1 Introduction

In recent years, Graph Neural Networks (GNNs) (Scarselli et al., 2008) have become ubiquitous in machine learning, emerging as the standard approach in many settings. For example, they have been successfully applied for tasks such as topic prediction in citation networks (Sen et al., 2008); molecule prediction (Gilmer et al., 2017); and link prediction in recommender systems (Wu et al., 2020a). These applications typically make use of message-passing GNNs (Gilmer et al., 2017), whose idea is fairly simple: in each layer, nodes are updated by aggregating the information (messages) coming from their neighboring nodes.

Depending on how this aggregation is implemented, we can define different types of GNN layers. Two important and widely adopted layers are graph convolutional networks (GCNs) (Kipf & Welling, 2017), which uniformly average the neighboring information; and graph attention networks (GATs) (Velickovic et al., 2018), which instead perform a weighted average, based on an attention score between receiver and sender nodes. More recently, a number of works have shown the strengths and limitations of both approaches from a theoretical (Fountoulakis et al., 2022; Baranwal et al., 2021, 2022), and empirical (Knyazev et al., 2019) point of view. These results show that their performance depends on the nature of the data at hand (i.e., the graph and the features), thus the standard approach is to select between GCNs and GATs via computationally demanding cross-validation.

In this work, we aim to exploit the benefits of both convolution and attention operations in the design of GNN architectures. To this end, we first introduce a novel graph convolutional attention layer (CAT), which extends existing attention layers by taking the convolved features as inputs of the score function. Following (Fountoulakis et al., 2022), we rely on a contextual stochastic block model to theoretically compare GCN, GAT, and CAT architectures. Our analysis shows that, unfortunately, no free lunch exists among these three GNN architectures since their performance, as expected, is fully data-dependent.

This motivates the main contribution of the paper, the *learnable graph convolutional attention network* (L-CAT): a novel GNN which, in each layer, automatically interpolates between the three operations by introducing only two scalar

*Equal contribution. Correspondence to: ajavaloy@cs.uni-saarland.de and psanchez@tue.mpg.de.

parameters. As a result, L-CAT is able to learn the proper operation to apply at each layer, thus combining different layer types in the same GNN architecture while overcoming the need to cross-validate—a process that was prohibitively expensive prior to this work. Our extensive empirical analysis demonstrates the capabilities of L-CAT on a wide range of datasets, outperforming existing baseline GNNs in terms of both performance, and robustness to input noise and network initialization.

2 Preliminaries

Assume as input an undirected graph $G = (V, E)$, where $V = [n]$ denotes the set of vertices of the graph, and $E \subseteq V \times V$ the set of edges. Each node $i \in [n]$ is represented by a d -dimensional feature vector $\mathbf{X}_i \in \mathbb{R}^d$, and the goal is to produce a set of predictions $\{\hat{\mathbf{y}}_i\}_{i=1}^n$.

To this end, a message-passing GNN layer yields a representation $\tilde{\mathbf{h}}_i \in \mathbb{R}^{d'}$ for each node i , by collecting and aggregating the information from each of its neighbors into a single message; and using the aggregated message to update its representation from the previous layer, $\mathbf{h}_i \in \mathbb{R}^d$. For the purposes of this work, we can define this operation as the following:

$$\tilde{\mathbf{h}}_i = f(\mathbf{h}'_i) \quad \text{where} \quad \mathbf{h}'_i \stackrel{\text{def}}{=} \sum_{j \in N_i^*} \gamma_{ij} \mathbf{W}_v \mathbf{h}_j, \quad (1)$$

where N_i^* is the set of neighbors of node i (including i), $\mathbf{W}_v \in \mathbb{R}^{d' \times d}$ a learnable matrix, f an elementwise function, and $\gamma_{ij} \in [0, 1]$ are coefficients such that $\sum_j \gamma_{ij} = 1$ for each node i .

Let the input features be $\mathbf{h}_i^0 = \mathbf{X}_i$, and $\mathbf{h}_i^L = \hat{\mathbf{y}}_i$ the predictions, then we can readily define a message-passing GNN (Gilmer et al., 2017) as a sequence of L layers as defined above. Depending on the way the coefficients γ_{ij} are computed, we identify different GNN flavors.

Graph convolutional networks (GCNs) (Kipf & Welling, 2017) are simple yet effective. In short, GCNs compute the average of the messages, i.e., they assign the same coefficient $\gamma_{ij} = 1/|N_i^*|$ to every neighbor:

$$\tilde{\mathbf{h}}_i = f(\mathbf{h}'_i) \quad \text{where} \quad \mathbf{h}'_i \stackrel{\text{def}}{=} \frac{1}{|N_i^*|} \sum_{j \in N_i^*} \mathbf{W}_v \mathbf{h}_j, \quad (2)$$

Graph attention networks take a different approach. Instead of assigning a fixed value to each coefficient γ_{ij} , they compute it as a function of the sender and receiver nodes. A general formulation for these models can be written as follows:

$$\tilde{\mathbf{h}}_i = f(\mathbf{h}'_i) \quad \text{where} \quad \mathbf{h}'_i \stackrel{\text{def}}{=} \sum_{j \in N_i^*} \gamma_{ij} \mathbf{W}_v \mathbf{h}_j \quad \text{and} \quad \gamma_{ij} \stackrel{\text{def}}{=} \frac{\exp(\Psi(\mathbf{h}_i, \mathbf{h}_j))}{\sum_{\ell \in N_i^*} \exp(\Psi(\mathbf{h}_i, \mathbf{h}_\ell))}. \quad (3)$$

Here, $\Psi(\mathbf{h}_i, \mathbf{h}_j) \stackrel{\text{def}}{=} \alpha(\mathbf{W}_q \mathbf{h}_i, \mathbf{W}_k \mathbf{h}_j)$ is known as the *score function* (or *attention architecture*), and provides a score value between the messages \mathbf{h}_i and \mathbf{h}_j (or more generally, between a learnable mapping of the messages). From these scores, the (attention) coefficients are obtained by normalizing them, such that $\sum_j \gamma_{ij} = 1$. We can find in the literature different attention layers and, throughout this work, we focus on the original GAT (Velickovic et al., 2018) and its extension GATv2 (Brody et al., 2022):

$$\text{GAT:} \quad \Psi(\mathbf{h}_i, \mathbf{h}_j) = \text{LeakyRelu}(\mathbf{a}^\top [\mathbf{W}_q \mathbf{h}_i \parallel \mathbf{W}_k \mathbf{h}_j]), \quad (4)$$

$$\text{GATv2:} \quad \Psi(\mathbf{h}_i, \mathbf{h}_j) = \mathbf{a}^\top \text{LeakyRelu}(\mathbf{W}_q \mathbf{h}_i + \mathbf{W}_k \mathbf{h}_j), \quad (5)$$

where the learnable parameters are now the attention vector \mathbf{a} ; and the matrices \mathbf{W}_q , \mathbf{W}_k , and \mathbf{W}_v . Following previous work (Velickovic et al., 2018; Brody et al., 2022), we assume that these matrices are coupled, i.e., $\mathbf{W}_q = \mathbf{W}_k = \mathbf{W}_v$. Note that the difference between the two layers lies in the position of the vector \mathbf{a} : by taking it out of the nonlinearity, Brody et al. (2022) increased the expressiveness of GATv2. Now, the product of \mathbf{a} and a weight matrix does not collapse into another vector. More importantly, the addition of two different attention layers will help us show the versatility of the proposed models later in §6.

3 Previous work

In recent years, there has been a surge of research in GNNs. Here, we discuss other GNN models, attention mechanisms, and the recent findings on the limitations of GCNs and GATs.

The literature on GNNs is extensive (Wu et al., 2020b; Hamilton et al., 2017a; Battaglia et al., 2018; Lee et al., 2019), and more abstract definitions of a message-passing GNN are possible, leading to other lines of work trying different ways to compute messages, aggregate them, or update the final message (Hamilton et al., 2017b; Xu et al., 2019; Corso et al., 2020). Alternatively, another line of work fully abandons message-passing, working instead with higher-order interactions (Morris et al., 2019). While some of this work is orthogonal—or directly applicable—to the proposed model, in the main paper we focus on convolutional and attention graph layers, as they are the most widely used (and cited) as of today.

While we consider the original GAT (Velickovic et al., 2018) and GATv2 (Brody et al., 2022), our work can be directly applied to any attention model that sticks to the formulation in Eq. 3. For example, some works propose different metrics for the score function, like the dot-product (Brody et al., 2022), cosine similarity (Thekumparampil et al., 2018), or a combination of various functions (Kim & Oh, 2021). Other works introduce transformer-based mechanisms (Vaswani et al., 2017) based on positional encoding (Dwivedi & Bresson, 2020; Kreuzer et al., 2021) or on the set transformer (Wang et al., 2021a). Finally, there also exist attention approaches designed for specific type of graphs, such as relational (Yun et al., 2019; Busbridge et al., 2019) or heterogeneous graphs (Wang et al., 2019b; Hu et al., 2020b).

3.1 On the limitations of GCN and GAT networks

Baranwal et al. (2021) studied classification on a simple stochastic block model, showing that, when the graph is neither too sparse nor noisy, applying one layer of graph convolution increases the regime in which the data is linearly separable. However, this result is highly sensitive to the graph structure, as convolutions essentially collapse the data to the same value in the presence of enough noise. More recently, Fountoulakis et al. (2022) showed that GAT is able to remedy the above issue, and provides perfect node separability regardless of the noise level in the graph. However, a classical argument (see Anderson (2003)) states that *in this particular setting* a linear classifier already achieves perfect separability. These works, in summary, showed scenarios for which GCNs can be beneficial in the absence of noise, and that GAT can outperform GCNs in other scenarios, leaving open the question of which architecture is preferable in terms of performance.

4 Convolved attention: benefits and hurdles

In this section, we propose to combine attention with convolution operations. To motivate it, we complement the results of Fountoulakis et al. (2022), providing a synthetic dataset for which *any* 1-layer GCN fails, but 1-layer GAT does not. Thus, proving a clear distinction between GAT and GCN layers. Besides, we show that convolution helps GAT as long as the graph noise is reasonable. The proofs for the two statements in this section appear in Appendix A and follow similar arguments as in Fountoulakis et al. (2022).

This dataset is based on the *contextual stochastic block model* (CSBM) (Deshpande et al., 2018). Let $\varepsilon_1, \dots, \varepsilon_n$ be iid. uniform samples from $\{-1, 0, 1\}$. Let $C_k = \{j \in [n] \mid \varepsilon_j = k\}$ for $k \in \{-1, 0, 1\}$. We set the feature vector $\mathbf{X}_i \sim \mathcal{N}(\varepsilon_i \boldsymbol{\mu}, \mathbf{I} \cdot \sigma^2)$ where $\boldsymbol{\mu} \in \mathbb{R}^d$, $\sigma \in \mathbb{R}$, and $\mathbf{I} \in \{0, 1\}^{d \times d}$ is the identity matrix. For a given pair $p, q \in [0, 1]$ we consider the stochastic adjacency matrix $\mathbf{A} \in \{0, 1\}^{n \times n}$ defined as follows: for $i, j \in [n]$ in the same class (*intra-edge*), we set $a_{ij} \sim \text{Ber}(p)$;² for i, j in different classes (*inter-edge*), we set $a_{ij} \sim \text{Ber}(q)$. We denote by $(\mathbf{X}, \mathbf{A}) \sim \text{CSBM}(n, p, q, \boldsymbol{\mu}, \sigma^2)$ a sample obtained according to the above random process. Our task is then to distinguish (or separate) nodes from C_0 vs. $C_{-1} \cup C_1$.

Note that, in general, it is impossible to separate C_0 from $C_{-1} \cup C_1$ with a linear classifier and, using one convolutional layer is detrimental for node classification on the CSBM:³ although the convolution brings the means closer and shrinks the variance, the geometric structure of the problem does not change. On the other hand, we prove that GAT is able to achieve perfect node separability when the graph is not too sparse:

Theorem 1. Suppose that $p, q = \Omega(\log^2 n/n)$ and $\|\boldsymbol{\mu}\|_2 = \omega(\sigma\sqrt{\log n})$. Then, there exists a choice of attention architecture Ψ such that, with probability at least $1 - o_n(1)$ over the data $(\mathbf{X}, \mathbf{A}) \sim \text{CSBM}(n, p, q, \boldsymbol{\mu}, \sigma^2)$, GAT separates nodes C_0 from $C_1 \cup C_{-1}$.

Moreover, we show using methods from Baranwal et al. (2021), that the above classification threshold $\|\boldsymbol{\mu}\|$ can be improved when the graph noise is reasonable. Specifically, *by applying convolution prior to the attention score*, the variance of the data is greatly reduced, and if the graph is not too noisy, the operation dramatically lowers the bound in

²Ber(\cdot) denote the Bernoulli distribution.

³We note that this problem can be easily solved by two layers of GCN (Baranwal et al., 2022).

Thm. 1. We exploit this insight by introducing the *graph convolutional attention layer* (CAT):

$$\Psi(\mathbf{h}_i, \mathbf{h}_j) = \alpha(\mathbf{W}\tilde{\mathbf{h}}_i, \mathbf{W}\tilde{\mathbf{h}}_j) \quad \text{where} \quad \tilde{\mathbf{h}}_i = \frac{1}{|N_i^*|} \sum_{\ell \in N_i^*} \mathbf{h}_\ell, \quad (6)$$

where $\tilde{\mathbf{h}}_i$ are the convolved features of the neighborhood of node i . As we show now, CAT improves over GAT by combining convolutions with attention, when the graph noise is low.

Corollary 2. Suppose $p, q = \Omega(\log^2 n/n)$ and $\|\boldsymbol{\mu}\| \geq \omega\left(\sigma\sqrt{\frac{(p+2q)\log n}{n(p-q)^2}}\right)$. Then, there is a choice of attention architecture Ψ such that CAT separates nodes C_0 from $C_1 \cup C_{-1}$, with probability at least $1 - o(1)$ over the data $(\mathbf{X}, \mathbf{A}) \sim \text{CSBM}(n, p, q, \boldsymbol{\mu}, \sigma^2)$.

The above proposition shows that under the CSBM data model, convolving prior to attention changes the regime for perfect node separability by a factor of $|p - q|\sqrt{n/(p + 2q)}$. This is desirable when $|p - q|\sqrt{n/(p + 2q)} > 1$, since the regime for perfect classification is increased. Otherwise, applying convolution prior to attention reduces the regime for perfect separability. Therefore, it is not always clear whether convolving prior to attention is beneficial.

5 L-CAT: Learning to interpolate

From the previous analysis, we can conclude that it is hard to know *a priori* whether attention, convolution, or convolved attention, will perform the best. In this section, we argue that this issue can be easily overcome by learning to interpolate between the three.

First, note that GCN and GAT only differ in that GCN weighs all neighbors equally (Eq. 2) and, the more similar the attention scores are (Eq. 3), the more uniform the coefficients γ_{ij} are. Thus, we can interpolate between GCN and GAT by introducing a learnable parameter. Similarly, the formulation of GAT (Eq. 3) and CAT (Eq. 6) differ in the convolution within the score, which can be interpolated with another learnable parameter.

Following this observation, we propose the *learnable convolutional attention layer* (L-CAT), which can be formulated as an attention layer with the following score:

$$\Psi(\mathbf{h}_i, \mathbf{h}_j) = \lambda_1 \cdot \alpha(\mathbf{W}\tilde{\mathbf{h}}_i, \mathbf{W}\tilde{\mathbf{h}}_j) \quad \text{where} \quad \tilde{\mathbf{h}}_i = \frac{\mathbf{h}_i + \lambda_2 \sum_{\ell \in N_i} \mathbf{h}_\ell}{1 + \lambda_2 |N_i|}, \quad (7)$$

where $\lambda_1, \lambda_2 \in [0, 1]$. As mentioned before, this formulation lets L-CAT learn to interpolate between GCN ($\lambda_1 = 0$), GAT ($\lambda_1 = 1$ and $\lambda_2 = 0$), and CAT ($\lambda_1 = 1$ and $\lambda_2 = 1$).

L-CAT enables a number of non-trivial benefits. Not only can it switch between existing layers, but it also learns the amount of attention necessary for each use-case. Moreover, by comprising the three layers in a single learnable formulation, it removes the necessity of cross-validating the type of layer, as their performance is data-dependent (see §§3.1 and 4). Remarkably, it allows to easily combine different layer types within the same architecture.

While we focus on GCN, L-CAT can be easily used with other GNN architectures such as PNA (Corso et al., 2020) and GCNII (Chen et al., 2020), as L-CAT interpolates between two different adjacency matrices. For further details and results, refer to App. F.

6 Experiments

In this section, we first validate our theoretical findings on synthetic data (§6.1). Then, we show through various node classification tasks that (L-)CAT is as competitive as the baseline models (§6.2). Lastly, we move to more demanding scenarios from the Open Graph Benchmark (Hu et al., 2020a), demonstrating that L-CAT is a more flexible and robust alternative to its baseline methods (§6.3) that reduces the need of cross-validating without giving up on performance. Refer to Apps. B to F for details and additional results. The code and scripts to reproduce our experiments can be found at <https://github.com/psanch21/L-CAT>.

6.1 Synthetic data

First, we empirically validate our theoretical results (Thm. 1 and Cor. 2). We aim to better understand the behavior of each layer as the properties of the data change, i.e., the noise level q (proportion of inter-edges) and the distance between the means of consecutive classes $\|\boldsymbol{\mu}\|$. We provide extra results and additional experiments in App. B.

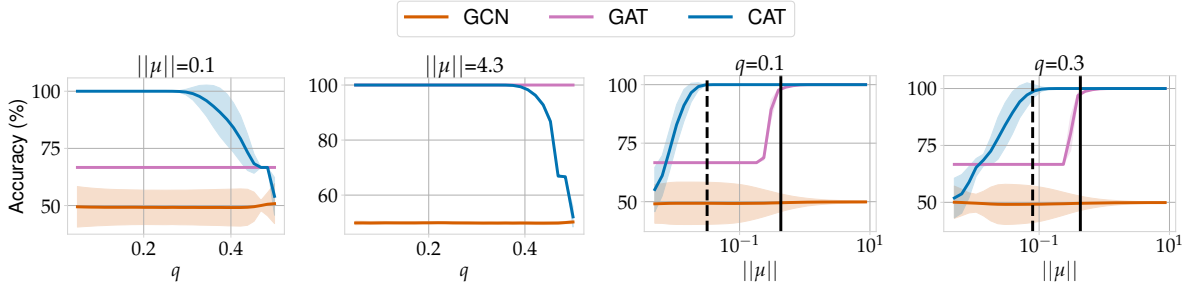


Figure 1: Synthetic data results. The left-most plots show accuracy as we vary the noise level q for $\|\mu\| = 0.1$ and $\|\mu\| = 4.3$. The right-most plots show the accuracy as we change the norm of the means $\|\mu\|$ for $q = 0.1$ and $q = 0.3$. We use two vertical lines to present the classification threshold stated in [Thm. 1](#) (solid line) and [Cor. 2](#) (dashed line).

Experimental setup. As data model, we use the proposed CSBM (see §4) with $n = 10000$, $p = 0.5$, $\sigma = 0.1$, and $d = n / (5 \log^2(n))$. All results are averaged over 50 runs, and parameters are set as described in [App. A](#). We conduct two experiments to assess the sensitivity to structural noise. First, we vary the noise level q between 0 and 0.5, leaving the mean vector μ fixed. We test two values of $\|\mu\|$: the first corresponds to the *easy* regime ($\|\mu\| = 10\sigma\sqrt{2\log n}$) where classes are far apart; and the second correspond to the *hard* regime ($\|\mu\| = \sigma$) where clusters are close. In the second experiment we instead sweep $\|\mu\|$ in the range $[\sigma/20, 20\sigma\sqrt{2\log n}]$, covering the transition from hard (small $\|\mu\|$) to easy (large $\|\mu\|$) settings. Here, we fix q to 0.1 (low noise) and 0.3 (high noise). In both cases, we compare the behavior of 1-layer GAT and CAT, and include GCN as the baseline.

Results. The two left-most plots of [Fig. 1](#) show node classification performance for the hard and easy regimes, respectively, as we vary the noise level q . In the hard regime, we observe that GAT is unable to achieve separation for any value of q , whereas CAT achieves perfect classification when q is small enough. This exemplifies the advantage of CAT over GAT as stated in [Cor. 2](#). When the distance between the means is large enough, we see that GAT achieves perfect results independently of q , as stated in [Thm. 1](#). In contrast, when CAT fails to satisfy the condition in [Cor. 2](#) (as we increase q), it achieves inferior performance.

The right-most part of [Fig. 1](#) shows the results when we fix q and sweep $\|\mu\|$. In these two plots, we can appreciate the transition in the accuracy of both GAT and CAT as a function of $\|\mu\|$. We observe that GAT achieves perfect accuracy when the distance between the means satisfies the condition in [Thm. 1](#) (solid vertical line in [Fig. 1](#)). Moreover, we can see the improvement CAT obtains over GAT. Indeed, when $\|\mu\|$ satisfies the conditions of [Cor. 2](#) (dashed vertical line in [Fig. 1](#)), the classification threshold is improved. As we increase q we see that the gap between the two vertical lines decreases, which means that the improvement of CAT over GAT decreases as q increments, exactly as stated in [Cor. 2](#).

6.2 Real data

We study now the performance of the proposed models in a comprehensive set of real-world experiments, in order to gain further insights of the settings in which they excel. Specifically, we found CAT and L-CAT to outperform their baselines as the average node degree increases. For a detailed description of the datasets and additional results, refer to [Apps. C, D](#) and [F](#).

Models. We consider as baselines a simple GCN layer ([Kipf & Welling, 2017](#)) where all neighbors are uniformly weighted, as well as the original GAT layer ([Velickovic et al., 2018](#)) and its recent extension, GATv2 ([Brody et al., 2022](#)). See §2 for an introduction. Based on the two attention models, we consider their CAT and L-CAT extensions. To ensure fair comparisons, all layers use the same number of parameters and share the same implementation, appropriately setting λ_1 and λ_2 (see [Eq. 7](#)) for each model.

Datasets. We consider six node classification datasets. The *Facebook/GitHub/TwitchEN* datasets involve social-network graphs ([Rozemberczki et al., 2021](#)), whose nodes represent verified pages/developers/streamers; and where the task is to predict the topic/expertise/explicit-language-use of the node. The *Coauthor Physics* dataset ([Shchur et al., 2018](#)) represents a co-authorship network whose nodes represent authors, and the task is to infer their main research field. The *Amazon* datasets represent two product-similarity graphs ([Shchur et al., 2018](#)), where each node is a product, and the task is to infer its category.

Experimental setup. To ensure the best results, we cross-validate all optimization-related hyperparameters for each model using GraphGym ([You et al., 2020](#)). All models use four GNN layers with hidden size of 32, and thus have

Table 1: Test accuracy (%) of the considered convolution and attention models for different datasets (sorted by their average node degree), and averaged over ten runs. Bold numbers are statistically different to their baseline model ($\alpha = 0.05$). Best average performance is underlined.

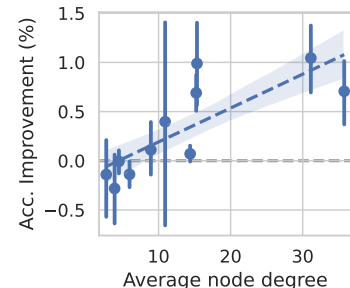
Dataset	<i>Amazon Computers</i>	<i>Amazon Photo</i>	<i>GitHub</i>	<i>Facebook PagePage</i>	<i>Coauthor Physics</i>	<i>TwitchEN</i>
Avg. Deg.	35.76	31.13	15.33	15.22	14.38	10.91
GCN	<u>90.59</u> \pm 0.36	<u>95.13</u> \pm 0.57	84.13 \pm 0.44	94.76 \pm 0.19	96.36 \pm 0.10	57.83 \pm 1.13
GAT	89.59 \pm 0.61	94.02 \pm 0.66	83.31 \pm 0.18	94.16 \pm 0.48	96.36 \pm 0.10	57.59 \pm 1.20
CAT	90.58 \pm 0.40	94.77 \pm 0.47	84.11 \pm 0.66	94.71 \pm 0.30	<u>96.40</u> \pm 0.10	58.09 \pm 1.61
L-CAT	90.34 \pm 0.47	94.93 \pm 0.37	84.05 \pm 0.70	<u>94.81</u> \pm 0.25	96.35 \pm 0.10	57.88 \pm 2.07
GATv2	89.49 \pm 0.53	93.47 \pm 0.62	82.92 \pm 0.45	93.44 \pm 0.30	96.24 \pm 0.19	57.70 \pm 1.17
CATv2	90.44 \pm 0.46	94.81 \pm 0.55	84.10 \pm 0.88	94.27 \pm 0.31	96.34 \pm 0.12	57.99 \pm 2.02
L-CATv2	90.33 \pm 0.44	94.79 \pm 0.61	<u>84.31</u> \pm 0.59	94.44 \pm 0.39	96.29 \pm 0.13	57.89 \pm 1.53

an equal number of parameters. For evaluation, we take the best-validation configuration during training, and report test-set performance. For further details, refer to App. D.

Results are presented in Table 1. In contrast with §6.1, we here find GCN to be a strong contender, reinforcing its viability in real-world data despite its simplicity. We observe both CAT and L-CAT not only holding up the performance with respect to their baselines models for all datasets, but in most cases also improving the test accuracy in a statistically significant manner. These results validate the effectiveness of CAT as a GNN layer, and show the viability of *L-CAT* as a *drop-in replacement*, achieving good results on all datasets.

As explained in §4, CAT differs from a usual GAT in that the score is computed with respect to the convolved features. Intuitively, this means that CAT should excel in those settings where nodes are better connected, allowing CAT to extract more information from their neighborhoods.

Indeed, in the inset figure we can observe the improvement in accuracy of CAT with respect to its baseline model, as a function of the average node degree of the dataset, and the linear regression fit of these results (dashed line). This plot includes all datasets (from the manuscript and App. D), and shows a positive trend between node connectivity and improved performance achieved by CAT.



6.3 Open Graph Benchmark

In this section, we assess the robustness of the proposed models, in order to fully understand their benefits. For further details and additional results, refer to App. E.

Datasets. We consider four datasets from the OGB suite (Hu et al., 2020a): *proteins*, *products*, *arxiv*, and *mag*. Note that these datasets are significantly larger than those from §6.2 and correspond to more difficult tasks, e.g., *arxiv* is a 40-class classification problem (see Table 5 in App. C for details). This makes them more suitable for the proposed analysis.

Experimental setup. We adopt the same experimental setup as Brody et al. (2022) for the *proteins*, *products*, and *mag* datasets. For the *arxiv* dataset, we use instead the example code from OGB (Hu et al., 2020a), as it yields better performance than that of Brody et al. (2022). Just as in §6.2, we compare with GCN (Kipf & Welling, 2017), GAT (Velickovic et al., 2018), GATv2 (Brody et al., 2022), and their CAT and L-CAT counterparts. We cross-validate the number of heads (1 and 8), and select the best-validation models during training. All models are identical except for their λ values.

Results are summarized in Table 2. Here we do not observe a clear preferred baseline: GCN performs really well in *proteins* and *mag*; GAT excels in *products*; and GATv2 does well in *arxiv* and *mag*. While CAT obtains the best results on *arxiv*, its performance on *proteins* and *products* is significantly worse than the baseline model. Presumably, an excessive amount of inter-edges could explain why convolving the features prior to computing the score is harmful, as seen in §6.1. As we explore in §6.3.2, however, CAT improves over its baseline for most *proteins* scenarios, specially with a single head. In stark contrast, L-CAT performs remarkably well, improving the baseline models in all datasets but *products*—even on those in which CAT fails—demonstrating the adaptability of L-CAT to different scenarios.

Table 2: Test performance of the considered models on four OGB datasets, averaged over five runs. Bold numbers are statistically different to their baseline model ($\alpha = 0.05$). Best average performance is underlined. Left table: accuracy (%); right table: AUC-ROC (%).

Dataset	<i>arxiv</i>	<i>products</i>	<i>mag</i>	<i>proteins</i>
GCN	71.58 \pm 0.20	74.12 \pm 1.20	<u>32.77 \pm 0.36</u>	<u>80.10 \pm 0.55</u>
GAT	71.58 \pm 0.16	78.53 \pm 0.91	32.15 \pm 0.31	79.08 \pm 1.47
CAT	<u>72.14 \pm 0.21</u>	<u>77.38 \pm 0.36</u>	31.98 \pm 0.46	73.26 \pm 1.65
L-CAT	<u>71.99 \pm 0.08</u>	77.19 \pm 1.11	32.47 \pm 0.38	79.63 \pm 0.71
GATv2	71.73 \pm 0.24	76.40 \pm 0.71	32.76 \pm 0.18	78.65 \pm 1.44
CATv2	<u>72.03 \pm 0.09</u>	74.81 \pm 1.12	<u>32.43 \pm 0.22</u>	74.33 \pm 0.94
L-CATv2	71.97 \pm 0.22	<u>76.37 \pm 0.92</u>	32.68 \pm 0.50	<u>79.07 \pm 0.98</u>

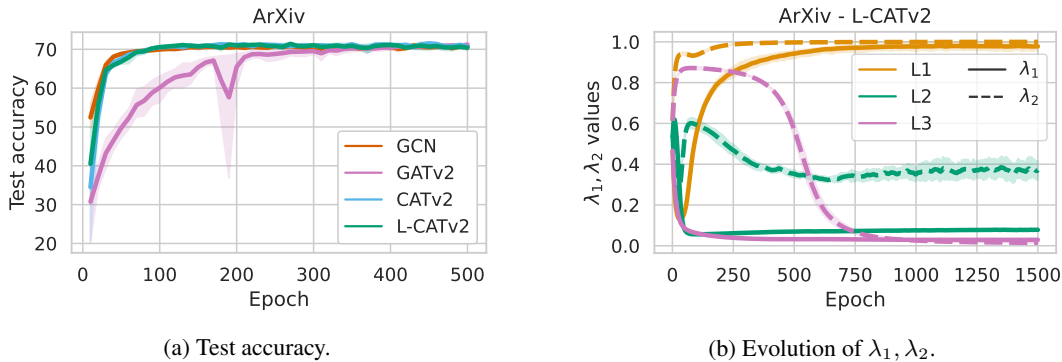


Figure 2: Behavior of GCN and GATv2-based models during training on the *arxiv* dataset. (a) CAT and L-CAT converge quicker and more stably than their baseline model. (b) L-CAT consistently converges to the same architecture: a CAT \rightarrow quasi-GCN \rightarrow GCN network.

To better understand the training dynamics of the models, we plot in Fig. 2a the test accuracy of GCN and the GATv2 models during training on the *arxiv* dataset. Interestingly, despite all models obtaining similar final results, *CATv2* and *L-CATv2* drastically improved their convergence speed and stability with respect to *GATv2*, matching that of GCN. To understand the behavior of L-CATv2, Fig. 2b shows the evolution of the λ parameters. We observe that, to achieve these results, L-CATv2 converged to a GNN network that combines three types of layers: the first layer is a CATv2 layer, taking advantage of the neighboring information; the second layer is a quasi-GCN layer, in which scores are almost uniform and some neighboring information is still used in the score computation; and the third layer is a pure GCN layer, in which all scores are uniformly distributed. It is important to remark that these dynamics are fairly consistent, as L-CATv2 reached the same λ values over all five runs.

6.3.1 Robustness to noise

One intrinsic aspect of real world data is the existence of noise. In this section, we explore the robustness of the proposed models to different levels of noise, i.e., we attempt to simulate scenarios where there exist measurement inaccuracies in the input features and edges.

Experimental setup. We consider the *arxiv* dataset, and the same experimental setup as in §6.3. We conduct two experiments. First, we introduce to the node features additive noise of the form $\mathcal{N}(\mathbf{0}, 1\sigma)$, and consider different levels of noise, $\sigma \in \{0, 0.25, 0.5, 0.75, 1\}$. Then, as in (Brody et al., 2022), we simulate edge noise by adding fake edges with probability $Bern(p)$ for $p \in \{0, 0.1, 0.2, 0.3, 0.4, 0.5\}$.

Results are shown in 3 for feature (3a) and edge noise (3b), summarizing the performance of all models over five runs and two numbers of heads (1 and 8). Baseline attention models are quite sensitive to feature noise, but are more robust to edge noise, as they can drop inter-class edges (see §3.1). GCNs, as expected, are instead more robust to feature noise, but suffer more in the presence of edge noise. In concordance with the synthetic experiments (see §§4 and 6.1), CAT is able to leverage convolutions as a variance-reduction technique, reducing the variance and improving its robustness to feature noise. Remarkably, L-CAT proves to be the most robust for both types of noise: by adapting the amount of attention used in each layer, it outperforms existing methods and reduces the variance.

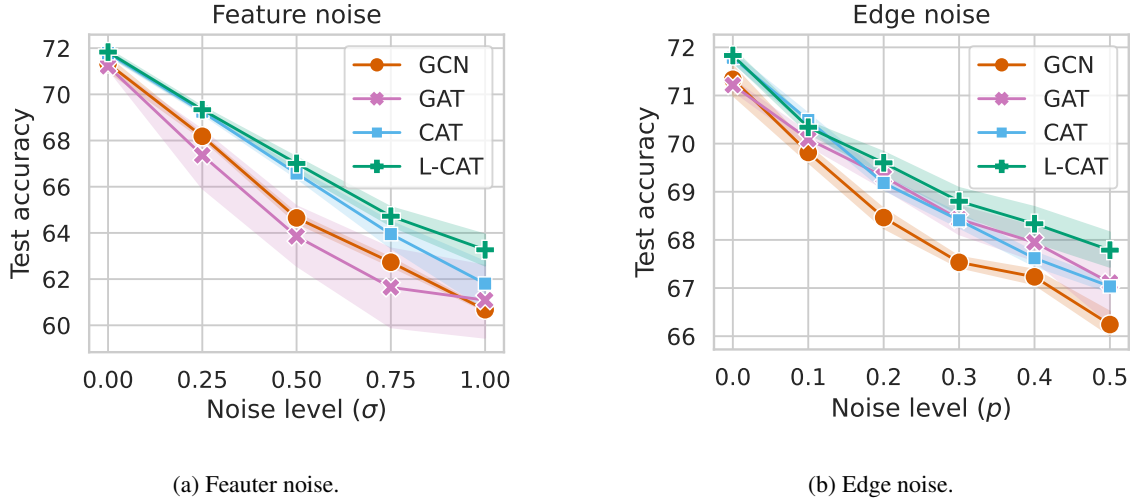


Figure 3: Robustness of CAT and L-CAT to (a) homoscedastic feature noise and (b) edge noise on the *arxiv* dataset.

Table 3: Test AUC-ROC (%) on the *proteins* dataset for attention models with two different network initializations (see §6.3.2), using 1 head (top) and 8 heads (bottom).

		GAT	CAT	L-CAT	GATv2	CATv2	L-CATv2
1h	<i>uniform</i>	59.73 ± 3.61	64.32 ± 2.33	77.77 ± 1.28	59.85 ± 2.73	64.32 ± 2.33	79.08 ± 0.95
	<i>normal</i>	66.38 ± 6.94	73.26 ± 1.65	78.06 ± 1.25	69.13 ± 8.48	74.33 ± 0.94	79.07 ± 0.98
8h	<i>uniform</i>	72.23 ± 2.86	73.60 ± 1.14	78.85 ± 1.57	75.21 ± 1.61	74.16 ± 1.30	78.77 ± 0.97
	<i>normal</i>	79.08 ± 1.47	74.67 ± 1.15	<u>79.63 ± 0.71</u>	78.65 ± 1.44	73.40 ± 0.56	79.30 ± 0.49
average		69.36 ± 8.52	73.93 ± 1.35	78.58 ± 1.48	70.71 ± 8.70	71.55 ± 4.54	<u>79.05 ± 0.91</u>

6.3.2 Robustness to network initialization

Another important aspect for real-world applications is robustness to network initialization, i.e., the ability to obtain satisfying performance independently of the initial parameters. Otherwise, a practitioner can waste lots of resources trying initializations or, even worse, give up on a model just because they did not try the initial parameters that yield great results.

Experimental setup. We follow once again the same setup for *proteins* as in §6.3. We consider two different network initializations. The first one, *uniform*, uses uniform Glorot initialization (Glorot & Bengio, 2010) with a gain of 1, which is the standard initialization used throughout this work. The second one, *normal*, uses instead normal Glorot initialization (Glorot & Bengio, 2010) with a gain of $\sqrt{2}$. This is the initialization employed on the original GATv2 paper (Brody et al., 2022) exclusively for the *proteins* dataset.

Results—segregated by number of heads—are shown in Table 3, while the results for GCN appear in the inset table. These results show that the baseline models perform poorly on the *uniform* initialization. However, this is somewhat alleviated when using 8 heads in the attention models. Moreover, all baselines significantly improve with *normal* initialization, being GCN the best model, and attention models obtaining 79% accuracy on average with 8 heads. Compared to the baselines, CAT does a good job and improves the performance in all cases except for *normal* with 8 heads. Remarkably, L-CAT consistently obtains high accuracy in all scenarios and runs. To emphasize consistency, bottom row shows the average accuracy across runs, showing that L-CAT is clearly more robust to parameter initialization than competing models.

GCN	
<i>uniform</i>	61.08 ± 2.56
<i>normal</i>	80.10 ± 0.55
average	70.59 ± 10.21

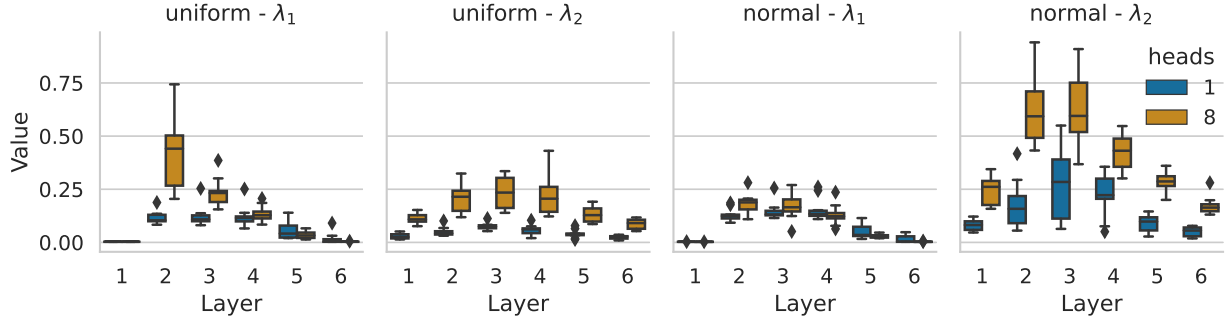


Figure 4: Distribution of λ_1, λ_2 on *proteins* dataset for L-CAT across initializations.

To understand this performance, we inspect the distribution of λ_1, λ_2 for L-CAT in Fig. 4. Here, we can spot a few interesting patterns. Consistently, the first and last layers are always GCNs, while the inner layers progressively admit less attention. Second, the number of heads affects the amount of attention allowed in the network; the more heads, the more expressive the layer tends to be, and more attention is permitted. Third, L-CAT adapts to the initialization used: in *uniform*, it allows more attention in the second layer; in *normal*, it allows more attention in the score inputs. These results consolidate the flexibility of L-CAT.

7 Conclusions and future work

In this work, we studied how to combine the strengths of convolution and attention layers in GNNs. We proposed CAT, which computes attention with respect to the convolved features, and analyzed its benefits and limitations on a new synthetic dataset. This analysis revealed different regimes where one model is preferred over the others, reinforcing the idea that selecting between GCNs, GATs, and now CATs, is a difficult task. For this reason, we proposed L-CAT, a model which interpolates between the three via two learnable parameters. Extensive experimental results demonstrated the effectiveness of L-CAT, yielding great results while being more robust than other methods. As a result, L-CAT proved to be a viable drop-in replacement that removes the need to cross-validate the layer type.

We strongly believe learnable interpolation can get us a long way, and we hope L-CAT to motivate new and exciting work. Specially, we are eager to see L-CAT in real applications, and thus finding out what combining different GNN layers across a model (without the hurdle of cross-validating all layer combinations) can lead to in the real-world.

8 Ethic statement

Given the nature of this work, we do not see any direct ethical concerns. On the contrary, L-CAT eases the application of GNNs to the practitioner, and removes the need of cross-validating the layer type, which can potentially benefit other areas and applications, as GNNs have already proven.

9 Reproducibility statement

For the theoretical results, we describe the data model used in §4, and provide all the detailed proofs in App. A. For the experimental results, we include in the supplementary material the necessary code and scripts required to reproduce our experiments, and all required datasets are freely available. Complete details about the experimental setup can be found in Apps. B, D and E, and we report in our results the mean and standard deviation computed using five trials or more. In addition, we highlight in bold the results that are statistically significant. Moreover, we include details of computational resources used for the all sets of experiments in App. B, App. D and App. E.

Acknowledgments

We would like to thank Batuhan Koyuncu, Jonas Kleesen, Miriam Rateike and Maryam Meghdadi Esfahani for helpful feedback and discussions. Pablo Sánchez Martín thanks the German Research Foundation through the Cluster of Excellence “Machine Learning – New Perspectives for Science”, EXC 2064/1, project number 390727645 for generous

funding support. The authors thank the International Max Planck Research School for Intelligent Systems (IMPRS-IS) for supporting Pablo Sánchez Martín.

References

- T.W. Anderson. *An introduction to multivariate statistical analysis*. 2003. (page 3)
- Jimmy Lei Ba, Jamie Ryan Kiros, and Geoffrey E Hinton. Layer normalization. *arXiv preprint arXiv:1607.06450*, 2016. (page 26)
- Aseem Baranwal, Kimon Fountoulakis, and Aukosh Jagannath. Graph convolution for semi-supervised classification: Improved linear separability and out-of-distribution generalization. In *International Conference on Machine Learning (ICML)*. PMLR, 2021. (page 1, 3, 14)
- Aseem Baranwal, Kimon Fountoulakis, and Aukosh Jagannath. Effects of graph convolutions in deep networks. *arXiv preprint arXiv:2204.09297*, 2022. (page 1, 3)
- Peter W Battaglia, Jessica B Hamrick, Victor Bapst, Alvaro Sanchez-Gonzalez, Vinicius Zambaldi, Mateusz Malinowski, Andrea Tacchetti, David Raposo, Adam Santoro, Ryan Faulkner, et al. Relational inductive biases, deep learning, and graph networks. *arXiv preprint arXiv:1806.01261*, 2018. (page 3)
- K. Bhatia, K. Dahiya, H. Jain, P. Kar, A. Mittal, Y. Prabhu, and M. Varma. The extreme classification repository: Multi-label datasets and code, 2016. (page 23)
- Aleksandar Bojchevski and Stephan Günnemann. Deep gaussian embedding of graphs: Unsupervised inductive learning via ranking. In *International Conference on Learning Representations (ICLR)*, 2018. (page 23)
- Shaked Brody, Uri Alon, and Eran Yahav. How attentive are graph attention networks? In *International Conference on Learning Representations (ICLR)*, 2022. (page 2, 3, 5, 6, 7, 8, 26, 27)
- Dan Busbridge, Dane Sherburn, Pietro Cavallo, and Nils Y Hammerla. Relational graph attention networks. *arXiv preprint arXiv:1904.05811*, 2019. (page 3)
- Ming Chen, Zhewei Wei, Zengfeng Huang, Bolin Ding, and Yaliang Li. Simple and deep graph convolutional networks. In *International Conference on Machine Learning (ICML)*, volume 119 of *Proceedings of Machine Learning Research*, 2020. (page 4, 28, 29, 30, 31)
- Gabriele Corso, Luca Cavalleri, Dominique Beaini, Pietro Liò, and Petar Velickovic. Principal neighbourhood aggregation for graph nets. In *Advances in Neural Information Processing Systems (NeurIPS)*, 2020. (page 3, 4, 28, 29, 30)
- Yash Deshpande, Subhabrata Sen, Andrea Montanari, and Elchanan Mossel. Contextual stochastic block models. In *Advances in Neural Information Processing Systems (NeurIPS)*, 2018. (page 3)
- Vijay Prakash Dwivedi and Xavier Bresson. A generalization of transformer networks to graphs. *arXiv preprint arXiv:2012.09699*, 2020. (page 3)
- Matthias Fey and Jan E. Lenssen. Fast graph representation learning with PyTorch Geometric. In *ICLR Workshop on Representation Learning on Graphs and Manifolds*, 2019. (page 25, 26)
- Kimon Fountoulakis, Amit Levi, Shenghao Yang, Aseem Baranwal, and Aukosh Jagannath. Graph attention retrospective. *arXiv preprint arXiv:2202.13060*, 2022. (page 1, 3, 14, 16, 17, 18)
- Justin Gilmer, Samuel S. Schoenholz, Patrick F. Riley, Oriol Vinyals, and George E. Dahl. Neural message passing for quantum chemistry. In *International Conference on Machine Learning (ICML)*, volume 70 of *Proceedings of Machine Learning Research*, 2017. (page 1, 2)
- Xavier Glorot and Yoshua Bengio. Understanding the difficulty of training deep feedforward neural networks. In *International Conference on Artificial Intelligence and Statistics (AISTATS)*, 2010. (page 8)
- William L. Hamilton, Rex Ying, and Jure Leskovec. Representation learning on graphs: Methods and applications. *IEEE Data Eng. Bull.*, 40, 2017a. (page 3)
- William L. Hamilton, Zhitao Ying, and Jure Leskovec. Inductive representation learning on large graphs. In *Advances in Neural Information Processing Systems (NeurIPS)*, 2017b. (page 3)
- Kaiming He, Xiangyu Zhang, Shaoqing Ren, and Jian Sun. Delving deep into rectifiers: Surpassing human-level performance on imagenet classification. In *IEEE International Conference on Computer Vision (ICCV)*, 2015. (page 24)

- Weihua Hu, Matthias Fey, Marinka Zitnik, Yuxiao Dong, Hongyu Ren, Bowen Liu, Michele Catasta, and Jure Leskovec. Open graph benchmark: Datasets for machine learning on graphs. In *Advances in Neural Information Processing Systems (NeurIPS)*, 2020a. (page 4, 6, 23, 26)
- Ziniu Hu, Yuxiao Dong, Kuansan Wang, and Yizhou Sun. Heterogeneous graph transformer. In *The Web Conference (WWW)*, 2020b. (page 3)
- Sergey Ioffe and Christian Szegedy. Batch normalization: Accelerating deep network training by reducing internal covariate shift. In *International Conference on Machine Learning (ICML)*, 2015. (page 24, 26)
- Dongkwan Kim and Alice Oh. How to find your friendly neighborhood: Graph attention design with self-supervision. In *International Conference on Learning Representations (ICLR)*, 2021. (page 3)
- Diederik P. Kingma and Jimmy Ba. Adam: A method for stochastic optimization. In *International Conference on Learning Representations (ICLR)*, 2015. (page 22, 24, 26)
- Thomas N. Kipf and Max Welling. Semi-supervised classification with graph convolutional networks. In *International Conference on Learning Representations (ICLR)*, 2017. (page 1, 2, 5, 6, 27, 28)
- Boris Knyazev, Graham W. Taylor, and Mohamed R. Amer. Understanding attention and generalization in graph neural networks. In *Advances in Neural Information Processing Systems (NeurIPS)*, 2019. (page 1)
- Devin Kreuzer, Dominique Beaini, Will Hamilton, Vincent Létourneau, and Prudencio Tossou. Rethinking graph transformers with spectral attention. *Advances in Neural Information Processing Systems (NeurIPS)*, 34, 2021. (page 3)
- John Boaz Lee, Ryan A Rossi, Sungchul Kim, Nesreen K Ahmed, and Eunye Koh. Attention models in graphs: A survey. *ACM Transactions on Knowledge Discovery from Data (TKDD)*, 13, 2019. (page 3)
- Christopher Morris, Martin Ritzert, Matthias Fey, William L. Hamilton, Jan Eric Lenssen, Gaurav Rattan, and Martin Grohe. Weisfeiler and leman go neural: Higher-order graph neural networks. In *Applications of Artificial Intelligence Conference (AAAI)*, 2019. (page 3)
- P. Rigollet and J.-C. Hütter. High dimensional statistics. *Lecture notes for course 18S997*, 813, 2015. (page 19)
- Benedek Rozemberczki, Carl Allen, and Rik Sarkar. Multi-scale attributed node embedding. *Journal of Complex Networks*, 2021. (page 5, 23)
- Franco Scarselli, Marco Gori, Ah Chung Tsoi, Markus Hagenbuchner, and Gabriele Monfardini. The graph neural network model. *IEEE transactions on neural networks*, 20, 2008. (page 1)
- Prithviraj Sen, Galileo Namata, Mustafa Bilgic, Lise Getoor, Brian Galligher, and Tina Eliassi-Rad. Collective classification in network data. *AI magazine*, 29(3), 2008. (page 1)
- Oleksandr Shchur, Maximilian Mumme, Aleksandar Bojchevski, and Stephan Günnemann. Pitfalls of graph neural network evaluation. *arXiv preprint arXiv:1811.05868*, 2018. (page 5, 23)
- Nitish Srivastava, Geoffrey Hinton, Alex Krizhevsky, Ilya Sutskever, and Ruslan Salakhutdinov. Dropout: A simple way to prevent neural networks from overfitting. *Journal of Machine Learning Research*, 15(56), 2014. (page 24, 26)
- Kiran K Thekumparampil, Chong Wang, Sewoong Oh, and Li-Jia Li. Attention-based graph neural network for semi-supervised learning. *arXiv preprint arXiv:1803.03735*, 2018. (page 3)
- Ashish Vaswani, Noam Shazeer, Niki Parmar, Jakob Uszkoreit, Llion Jones, Aidan N. Gomez, Lukasz Kaiser, and Illia Polosukhin. Attention is all you need. In *Advances in Neural Information Processing Systems (NeurIPS)*, 2017. (page 3)
- Petar Velickovic, Guillem Cucurull, Arantxa Casanova, Adriana Romero, Pietro Liò, and Yoshua Bengio. Graph attention networks. In *International Conference on Learning Representations (ICLR)*, 2018. (page 1, 2, 3, 5, 6, 27)
- Guangtao Wang, Rex Ying, Jing Huang, and Jure Leskovec. Multi-hop attention graph neural networks. In *International Joint Conference on Artificial Intelligence (IJCAI)*, 2021a. (page 3)
- Kuansan Wang, Zhihong Shen, Chiyuan Huang, Chieh-Han Wu, Yuxiao Dong, and Anshul Kanakia. Microsoft academic graph: When experts are not enough. *Quantitative Science Studies*, 2020. (page 23, 24)
- Minjie Wang, Da Zheng, Zihao Ye, Quan Gan, Mufei Li, Xiang Song, Jinjing Zhou, Chao Ma, Lingfan Yu, Yu Gai, Tianjun Xiao, Tong He, George Karypis, Jinyang Li, and Zheng Zhang. Deep graph library: A graph-centric, highly-performant package for graph neural networks. *arXiv preprint arXiv:1909.01315*, 2019a. (page 26)
- Xiao Wang, Houye Ji, Chuan Shi, Bai Wang, Yanfang Ye, Peng Cui, and Philip S. Yu. Heterogeneous graph attention network. In *The World Wide Web Conference, WWW 2019, San Francisco, CA, USA, May 13-17, 2019*, 2019b. (page 3)

- Yangkun Wang, Jiarui Jin, Weinan Zhang, Yong Yu, Zheng Zhang, and David Wipf. Bag of tricks for node classification with graph neural networks. *arXiv preprint arXiv:2103.13355*, 2021b. (page 28)
- Shiwen Wu, Fei Sun, Wentao Zhang, Xu Xie, and Bin Cui. Graph neural networks in recommender systems: a survey. *ACM Computing Surveys (CSUR)*, 2020a. (page 1)
- Zonghan Wu, Shirui Pan, Fengwen Chen, Guodong Long, Chengqi Zhang, and S Yu Philip. A comprehensive survey on graph neural networks. *IEEE transactions on neural networks and learning systems*, 32, 2020b. (page 3)
- Keyulu Xu, Weihua Hu, Jure Leskovec, and Stefanie Jegelka. How powerful are graph neural networks? In *International Conference on Learning Representations (ICLR)*, 2019. (page 3, 28)
- Zhilin Yang, William W. Cohen, and Ruslan Salakhutdinov. Revisiting semi-supervised learning with graph embeddings. In *International Conference on Machine Learning (ICML)*, volume 48 of *JMLR Workshop and Conference Proceedings*, 2016. (page 23)
- Jiaxuan You, Zhitao Ying, and Jure Leskovec. Design space for graph neural networks. *Advances in Neural Information Processing Systems (NeurIPS)*, 33, 2020. (page 5, 24)
- Seongjun Yun, Minbyul Jeong, Raehyun Kim, Jaewoo Kang, and Hyunwoo J. Kim. Graph transformer networks. In *Advances in Neural Information Processing Systems (NeurIPS)*, 2019. (page 3)

Appendix

Table of Contents

A	Theoretical results	14
A.1	A hard example for GCN	14
A.2	A solution for GAT and CAT	15
B	Synthetic experiments	20
B.1	Other experiments	22
C	Dataset description	23
D	Real data experiments	24
D.1	Experimental details	24
D.2	Additional results	25
E	Open Graph Benchmark experiments	26
E.1	Experimental details	26
E.2	Additional results	26
F	Extending L-CAT to other GNN models	28
F.1	PNA experiments	28
F.2	GCNII experiments	29

A Theoretical results

A.1 A hard example for GCN

In this subsection, we present a dataset and classification task for which GCN performs poorly. Note that we follow the similar techniques and notation as (Fountoulakis et al., 2022), as described in the main paper.

We recall our data model. Fix $n, d \in \mathbb{N}$ and let $\varepsilon_1, \dots, \varepsilon_n$ be i.i.d uniformly sampled from $\{-1, 0, 1\}$. Let $C_k = \{j \in [n] \mid \varepsilon_j = k\}$ for $k \in \{-1, 0, 1\}$. For each index $i \in [n]$, we set the feature vector $\mathbf{X}_i \in \mathbb{R}^d$ as $\mathbf{X}_i \sim \mathcal{N}(\varepsilon_i \cdot \boldsymbol{\mu}, \mathbf{I} \cdot \sigma^2)$, where $\boldsymbol{\mu} \in \mathbb{R}^d$, $\sigma \in \mathbb{R}$ and $\mathbf{I} \in \{0, 1\}^{d \times d}$ is the identity matrix. For a given pair $p, q \in [0, 1]$ we consider the stochastic adjacency matrix $\mathbf{A} \in \{0, 1\}^{n \times n}$ defined as follows. For $i, j \in [n]$ in the same class, we set $a_{ij} \sim \text{Ber}(p)$, and if i, j are in different classes, we set $a_{ij} \sim \text{Ber}(q)$. We let $\mathbf{D} \in \mathbb{R}^{n \times n}$ be a diagonal matrix containing the degrees of the vertices. We denote by $(\mathbf{X}, \mathbf{A}) \sim \text{CSBM}(n, p, q, \boldsymbol{\mu}, \sigma^2)$ a sample obtained according to the above random process.

The task we wish to solve is classifying C_0 vs $C_{-1} \cup C_1$. Namely, we want our model φ to satisfy $\varphi(\mathbf{X}_i) < 0$ if and only if $i \in C_0$. Moreover, note that the posed problem is *not linearly classifiable*.

To this end, we start by stating an assumption on the choice of parameters. This assumption is necessary to achieve degree concentration in the graph.

Assumption 1. $p, q = \Omega(\log^2 n/n)$.

We now show the distribution of the convolved features. The following lemma can be easily obtained using the techniques in Baranwal et al. (2021).

Lemma 3. Fix p, q satisfying Assumption 1. With probability at least $1 - o(1)$ over \mathbf{A} and $\{\varepsilon_i\}_i$,

$$(\mathbf{D}^{-1} \mathbf{A} \mathbf{X})_i \sim \mathcal{N}\left(\varepsilon_i \cdot \frac{p-q}{p+2q} \boldsymbol{\mu}, \frac{\sigma^2}{n(p+2q)}\right), \quad \forall i \in [n].$$

To prove the above lemma, we need the following definition of our high probability event.

Definition 1. We define the event \mathcal{E} as the intersection of the following events over \mathbf{A} and $\{\varepsilon_i\}_i$:

1. \mathcal{E}_1 is the event that $|C_0| = \frac{n}{3} \pm O(\sqrt{n \log n})$, $|C_1| = \frac{n}{3} \pm O(\sqrt{n \log n})$ and $|C_{-1}| = \frac{n}{3} \pm O(\sqrt{n \log n})$.
2. \mathcal{E}_2 is the event that for each $i \in [n]$, $\mathbf{D}_{ii} = \frac{n(p+2q)}{3} \left(1 \pm \frac{10}{\sqrt{\log n}}\right)$.
3. \mathcal{E}_3 is the event that for each $i \in [n]$ and $k \in \{-1, 0, 1\}$,

$$|N_i \cap C_k| = \begin{cases} \mathbf{D}_{ii} \cdot \frac{p}{p+2q} \cdot \left(1 \pm \frac{10}{\sqrt{\log n}}\right) & \text{if } i \in C_k \\ \mathbf{D}_{ii} \cdot \frac{q}{p+2q} \cdot \left(1 \pm \frac{10}{\sqrt{\log n}}\right) & \text{if } i \notin C_k \end{cases}.$$

The following lemma is a direct application of Chernoff bound and a union bound.

Lemma 4. With probability at least $1 - 1/\text{poly}(n)$ the event \mathcal{E} holds.

Proof of Lemma 3. By applying Lemma 4, and conditioned on \mathcal{E} , for any $i \in [n]$

$$(\mathbf{D}^{-1} \mathbf{A} \mathbf{X})_i = \frac{1}{\mathbf{D}_{ii}} \sum_{j \in N_i} \mathbf{X}_j = \frac{1}{\mathbf{D}_{ii}} \left(\sum_{j \in N_i \cap C_{-1}} \mathbf{X}_j + \sum_{j \in N_i \cap C_0} \mathbf{X}_j + \sum_{j \in N_i \cap C_1} \mathbf{X}_j \right).$$

Using the definition of \mathcal{E} and properties of Gaussian distributions the lemma follows. \square

Lemma 3 shows that essentially, the convolution reduced the variance and moved the means closer, but the structure of the problem stayed exactly the same. Therefore, one layer of GCN cannot separate C_0 from $C_{-1} \cup C_1$ with high probability.

A.2 A solution for GAT and CAT

In what follows, we show that GAT is able to handle the above classification task easily when the distance between the means is large enough. Then, we show how the additional convolution on the inputs to the score function improves the regime of perfect classification when the graph is not too noisy. Our main technical lemma considers a specific attention architecture and characterize the attention scores for our data model.

Lemma 5. Suppose that p, q satisfy [Assumption 1](#), $\|\boldsymbol{\mu}\| \geq \omega(\sigma\sqrt{\log n})$, fix the LeakyRelu constant $\beta \in (0, 1)$ and $R \in \mathbb{R}$. Then, there exists a choice of attention architecture Ψ such that with probability at least $1 - o_n(1)$ over the data $(\mathbf{X}, \mathbf{A}) \sim \text{CSBM}(n, p, q, \boldsymbol{\mu}, \sigma^2)$ the following holds.

$$\Psi(\mathbf{X}_i, \mathbf{X}_j) = \begin{cases} 10R\beta\|\boldsymbol{\mu}\|(1 \pm o(1)) & \text{if } i, j \in C_1^2 \\ -2R\|\boldsymbol{\mu}\|(1 + 2\beta)(1 \pm o(1)) & \text{if } i, j \in C_{-1}^2 \\ -2R\|\boldsymbol{\mu}\|(1 + 5\beta)(1 \pm o(1)) & \text{if } i \in C_1, j \in C_{-1} \\ 10R\beta\|\boldsymbol{\mu}\|(1 \pm o(1)) & \text{if } i \in C_{-1}, j \in C_1 \\ -\frac{R}{2}\|\boldsymbol{\mu}\|(1 - 21\beta)(1 \pm o(1)) & \text{if } i \in C_0, j \in C_1 \\ -\frac{R}{2}\|\boldsymbol{\mu}\|(1 - 11\beta)(1 \pm o(1)) & \text{if } i \in C_0, j \in C_{-1} \\ -\frac{R}{2}\|\boldsymbol{\mu}\|(1 - 5\beta)(1 \pm o(1)) & \text{if } i \in C_1, j \in C_0 \\ -\frac{R}{2}\|\boldsymbol{\mu}\|(1 - 5\beta)(1 \pm o(1)) & \text{if } i \in C_{-1}, j \in C_0 \\ 2R\beta\|\boldsymbol{\mu}\|(1 \pm o(1)) & \text{if } i, j \in C_0^2 \end{cases}.$$

Proof. We consider as an ansatz the following two layer architecture Ψ .

$$\tilde{\mathbf{w}} \stackrel{\text{def}}{=} \frac{\boldsymbol{\mu}}{\|\boldsymbol{\mu}\|}, \quad \mathbf{S} \stackrel{\text{def}}{=} \begin{bmatrix} 1 & 1 \\ -1 & -1 \\ 1 & -1 \\ -1 & 1 \\ 0 & 1 \\ 1 & 0 \\ 0 & -1 \\ -1 & 0 \end{bmatrix}, \quad \mathbf{b} \stackrel{\text{def}}{=} \begin{bmatrix} -3/2 \\ -3/2 \\ -3/2 \\ -3/2 \\ -1/2 \\ -1/2 \\ -1/2 \\ -1/2 \end{bmatrix} \cdot \|\boldsymbol{\mu}\|, \quad \mathbf{r} \stackrel{\text{def}}{=} R \cdot \begin{bmatrix} 2 \\ -2 \\ -2 \\ 2 \\ -1 \\ -1 \\ -1 \\ -1 \end{bmatrix},$$

where $R > 0$ is an arbitrary scaling parameter. The output of the attention model is defined as

$$\Psi(\mathbf{X}_i, \mathbf{X}_j) \stackrel{\text{def}}{=} \mathbf{r}^T \cdot \text{LeakyRelu} \left(\mathbf{S} \cdot \begin{bmatrix} \tilde{\mathbf{w}}^T \mathbf{X}_i \\ \tilde{\mathbf{w}}^T \mathbf{X}_j \end{bmatrix} + \mathbf{b} \right).$$

Let $\boldsymbol{\Delta}_{ij} \stackrel{\text{def}}{=} \mathbf{S} \cdot \begin{bmatrix} \tilde{\mathbf{w}}^T \mathbf{X}_i \\ \tilde{\mathbf{w}}^T \mathbf{X}_j \end{bmatrix} + \mathbf{b} \in \mathbb{R}^8$, and note that for each element $t \in [8]$ of $\boldsymbol{\Delta}_{ij}$, we have that $(\boldsymbol{\Delta}_{ij})_t = \mathbf{S}_{t,1}\tilde{\mathbf{w}}^T \mathbf{X}_i + \mathbf{S}_{t,2}\tilde{\mathbf{w}}^T \mathbf{X}_j + \mathbf{b}_t$. Note that the random variable $(\boldsymbol{\Delta}_{ij})_t$ is distributed as follows:

$$(\boldsymbol{\Delta}_{ij})_t \sim \begin{cases} \mathcal{N}((\mathbf{S}_{t,1} + \mathbf{S}_{t,2})\tilde{\mathbf{w}}^T \boldsymbol{\mu} + \mathbf{b}_t, \|\mathbf{S}_{t,*}\|^2 \sigma^2) & \text{if } i, j \in C_1^2 \\ \mathcal{N}(-(\mathbf{S}_{t,1} + \mathbf{S}_{t,2})\tilde{\mathbf{w}}^T \boldsymbol{\mu} + \mathbf{b}_t, \|\mathbf{S}_{t,*}\|^2 \sigma^2) & \text{if } i, j \in C_{-1}^2 \\ \mathcal{N}((\mathbf{S}_{t,1} - \mathbf{S}_{t,2})\tilde{\mathbf{w}}^T \boldsymbol{\mu} + \mathbf{b}_t, \|\mathbf{S}_{t,*}\|^2 \sigma^2) & \text{if } i \in C_1, j \in C_{-1} \\ \mathcal{N}(-(\mathbf{S}_{t,1} - \mathbf{S}_{t,2})\tilde{\mathbf{w}}^T \boldsymbol{\mu} + \mathbf{b}_t, \|\mathbf{S}_{t,*}\|^2 \sigma^2) & \text{if } i \in C_{-1}, j \in C_1 \\ \mathcal{N}(\mathbf{S}_{t,2}\tilde{\mathbf{w}}^T \boldsymbol{\mu} + \mathbf{b}_t, \|\mathbf{S}_{t,*}\|^2 \sigma^2) & \text{if } i \in C_0, j \in C_1 \\ \mathcal{N}(-\mathbf{S}_{t,2}\tilde{\mathbf{w}}^T \boldsymbol{\mu} + \mathbf{b}_t, \|\mathbf{S}_{t,*}\|^2 \sigma^2) & \text{if } i \in C_0, j \in C_{-1} \\ \mathcal{N}(\mathbf{S}_{t,1}\tilde{\mathbf{w}}^T \boldsymbol{\mu} + \mathbf{b}_t, \|\mathbf{S}_{t,*}\|^2 \sigma^2) & \text{if } i \in C_1, j \in C_0 \\ \mathcal{N}(-\mathbf{S}_{t,1}\tilde{\mathbf{w}}^T \boldsymbol{\mu} + \mathbf{b}_t, \|\mathbf{S}_{t,*}\|^2 \sigma^2) & \text{if } i \in C_{-1}, j \in C_0 \\ \mathcal{N}(\mathbf{b}_t, \|\mathbf{S}_{t,*}\|^2 \sigma^2) & \text{if } i, j \in C_0^2 \end{cases}.$$

Therefore, for a fixed $i, j \in [n]^2$ we have that the entries of $\boldsymbol{\Delta}_{ij}$ are distributed as follows (where we use \mathcal{N}_x^y as abbreviation for the Gaussian $\mathcal{N}(x, y)$)

$$\begin{aligned} & \left[\mathcal{N}_{\frac{\|\boldsymbol{\mu}\|}{2}}^{4\sigma^2} \quad \mathcal{N}_{-\frac{7\|\boldsymbol{\mu}\|}{2}}^{4\sigma^2} \quad \mathcal{N}_{-\frac{3\|\boldsymbol{\mu}\|}{2}}^{4\sigma^2} \quad \mathcal{N}_{-\frac{3\|\boldsymbol{\mu}\|}{2}}^{4\sigma^2} \quad \mathcal{N}_{\frac{\|\boldsymbol{\mu}\|}{2}}^{\sigma^2} \quad \mathcal{N}_{\frac{\|\boldsymbol{\mu}\|}{2}}^{\sigma^2} \quad \mathcal{N}_{-\frac{3\|\boldsymbol{\mu}\|}{2}}^{\sigma^2} \quad \mathcal{N}_{-\frac{3\|\boldsymbol{\mu}\|}{2}}^{\sigma^2} \right] \quad \text{for } i, j \in C_1^2, \\ & \left[\mathcal{N}_{-\frac{7\|\boldsymbol{\mu}\|}{2}}^{4\sigma^2} \quad \mathcal{N}_{\frac{\|\boldsymbol{\mu}\|}{2}}^{4\sigma^2} \quad \mathcal{N}_{-\frac{3\|\boldsymbol{\mu}\|}{2}}^{4\sigma^2} \quad \mathcal{N}_{-\frac{3\|\boldsymbol{\mu}\|}{2}}^{4\sigma^2} \quad \mathcal{N}_{-\frac{3\|\boldsymbol{\mu}\|}{2}}^{\sigma^2} \quad \mathcal{N}_{-\frac{3\|\boldsymbol{\mu}\|}{2}}^{\sigma^2} \quad \mathcal{N}_{\frac{\|\boldsymbol{\mu}\|}{2}}^{\sigma^2} \quad \mathcal{N}_{\frac{\|\boldsymbol{\mu}\|}{2}}^{\sigma^2} \right] \quad \text{for } i, j \in C_{-1}^2, \end{aligned}$$

$$\begin{aligned}
& \left[\mathcal{N}_{-\frac{3\|\mu\|}{2}}^{4\sigma^2} \quad \mathcal{N}_{-\frac{3\|\mu\|}{2}}^{4\sigma^2} \quad \mathcal{N}_{\frac{\|\mu\|}{2}}^{4\sigma^2} \quad \mathcal{N}_{-\frac{7\|\mu\|}{2}}^{4\sigma^2} \quad \mathcal{N}_{-\frac{3\|\mu\|}{2}}^{\sigma^2} \quad \mathcal{N}_{\frac{\|\mu\|}{2}}^{\sigma^2} \quad \mathcal{N}_{\frac{\|\mu\|}{2}}^{\sigma^2} \quad \mathcal{N}_{-\frac{3\|\mu\|}{2}}^{\sigma^2} \right] & \text{for } i, j \in C_1 \times C_{-1}, \\
& \left[\mathcal{N}_{-\frac{3\|\mu\|}{2}}^{4\sigma^2} \quad \mathcal{N}_{-\frac{3\|\mu\|}{2}}^{4\sigma^2} \quad \mathcal{N}_{-\frac{7\|\mu\|}{2}}^{4\sigma^2} \quad \mathcal{N}_{\frac{\|\mu\|}{2}}^{4\sigma^2} \quad \mathcal{N}_{\frac{\|\mu\|}{2}}^{\sigma^2} \quad \mathcal{N}_{-\frac{3\|\mu\|}{2}}^{\sigma^2} \quad \mathcal{N}_{-\frac{3\|\mu\|}{2}}^{\sigma^2} \quad \mathcal{N}_{\frac{\|\mu\|}{2}}^{\sigma^2} \right] & \text{for } i, j \in C_{-1} \times C_1, \\
& \left[\mathcal{N}_{-\frac{\|\mu\|}{2}}^{4\sigma^2} \quad \mathcal{N}_{-\frac{5\|\mu\|}{2}}^{4\sigma^2} \quad \mathcal{N}_{-\frac{5\|\mu\|}{2}}^{4\sigma^2} \quad \mathcal{N}_{-\frac{5\|\mu\|}{2}}^{4\sigma^2} \quad \mathcal{N}_{\frac{\|\mu\|}{2}}^{\sigma^2} \quad \mathcal{N}_{-\frac{\|\mu\|}{2}}^{\sigma^2} \quad \mathcal{N}_{-\frac{3\|\mu\|}{2}}^{\sigma^2} \quad \mathcal{N}_{-\frac{\|\mu\|}{2}}^{\sigma^2} \right] & \text{for } i, j \in C_0 \times C_1, \\
& \left[\mathcal{N}_{-\frac{5\|\mu\|}{2}}^{4\sigma^2} \quad \mathcal{N}_{-\frac{\|\mu\|}{2}}^{4\sigma^2} \quad \mathcal{N}_{-\frac{\|\mu\|}{2}}^{4\sigma^2} \quad \mathcal{N}_{-\frac{5\|\mu\|}{2}}^{4\sigma^2} \quad \mathcal{N}_{-\frac{3\|\mu\|}{2}}^{\sigma^2} \quad \mathcal{N}_{-\frac{\|\mu\|}{2}}^{\sigma^2} \quad \mathcal{N}_{\frac{\|\mu\|}{2}}^{\sigma^2} \quad \mathcal{N}_{-\frac{\|\mu\|}{2}}^{\sigma^2} \right] & \text{for } i, j \in C_0 \times C_{-1}, \\
& \left[\mathcal{N}_{-\frac{\|\mu\|}{2}}^{4\sigma^2} \quad \mathcal{N}_{-\frac{5\|\mu\|}{2}}^{4\sigma^2} \quad \mathcal{N}_{-\frac{\|\mu\|}{2}}^{4\sigma^2} \quad \mathcal{N}_{-\frac{5\|\mu\|}{2}}^{4\sigma^2} \quad \mathcal{N}_{-\frac{\|\mu\|}{2}}^{\sigma^2} \quad \mathcal{N}_{\frac{\|\mu\|}{2}}^{\sigma^2} \quad \mathcal{N}_{-\frac{\|\mu\|}{2}}^{\sigma^2} \quad \mathcal{N}_{-\frac{3\|\mu\|}{2}}^{\sigma^2} \right] & \text{for } i, j \in C_1 \times C_0, \\
& \left[\mathcal{N}_{-\frac{5\|\mu\|}{2}}^{4\sigma^2} \quad \mathcal{N}_{-\frac{\|\mu\|}{2}}^{4\sigma^2} \quad \mathcal{N}_{-\frac{5\|\mu\|}{2}}^{4\sigma^2} \quad \mathcal{N}_{-\frac{\|\mu\|}{2}}^{4\sigma^2} \quad \mathcal{N}_{-\frac{\|\mu\|}{2}}^{\sigma^2} \quad \mathcal{N}_{-\frac{3\|\mu\|}{2}}^{\sigma^2} \quad \mathcal{N}_{-\frac{\|\mu\|}{2}}^{\sigma^2} \quad \mathcal{N}_{\frac{\|\mu\|}{2}}^{\sigma^2} \right] & \text{for } i, j \in C_{-1} \times C_0, \\
& \left[\mathcal{N}_{-\frac{3\|\mu\|}{2}}^{4\sigma^2} \quad \mathcal{N}_{-\frac{3\|\mu\|}{2}}^{4\sigma^2} \quad \mathcal{N}_{-\frac{3\|\mu\|}{2}}^{4\sigma^2} \quad \mathcal{N}_{-\frac{3\|\mu\|}{2}}^{4\sigma^2} \quad \mathcal{N}_{-\frac{\|\mu\|}{2}}^{\sigma^2} \quad \mathcal{N}_{-\frac{3\|\mu\|}{2}}^{\sigma^2} \quad \mathcal{N}_{-\frac{\|\mu\|}{2}}^{\sigma^2} \quad \mathcal{N}_{-\frac{\|\mu\|}{2}}^{\sigma^2} \right] & \text{for } i, j \in C_0^2,
\end{aligned}$$

Next, we will use the following lemma regarding LeakyRelu concentration.

Lemma 6 (Lemma A.6 in [Fountoulakis et al. \(2022\)](#)). Fix $s \in \mathbb{N}$, and let z_1, \dots, z_s be jointly Gaussian random variables with marginals $z_i \sim \mathcal{N}(\mu_i, \sigma_i^2)$. There exists an absolute constant $C > 0$ such that with probability at least $1 - o_s(1)$, we have

$$\text{LeakyRelu}(z_i) = \text{LeakyRelu}(\mu_i) \pm C\sigma_i\sqrt{\log s}, \quad \text{for all } i \in [s].$$

Using [Lemma 6](#) with the assumption on $\|\mu\|$ and a union bound, we have that with probability at least $1 - o_n(1)$, $\text{LeakyRelu}(\Delta_{ij})$ is (up to $1 \pm o(1)$)

$$\begin{aligned}
& \left[\frac{\|\mu\|}{2} \quad \frac{-7\beta\|\mu\|}{2} \quad \frac{-3\beta\|\mu\|}{2} \quad \frac{-3\beta\|\mu\|}{2} \quad \frac{\|\mu\|}{2} \quad \frac{\|\mu\|}{2} \quad \frac{-3\beta\|\mu\|}{2} \quad \frac{-3\beta\|\mu\|}{2} \right] & \text{for } i, j \in C_1^2, \\
& \left[\frac{-7\beta\|\mu\|}{2} \quad \frac{\|\mu\|}{2} \quad \frac{-3\beta\|\mu\|}{2} \quad \frac{-3\beta\|\mu\|}{2} \quad \frac{-3\beta\|\mu\|}{2} \quad \frac{-3\beta\|\mu\|}{2} \quad \frac{\|\mu\|}{2} \quad \frac{\|\mu\|}{2} \right] & \text{for } i, j \in C_{-1}^2, \\
& \left[\frac{-3\beta\|\mu\|}{2} \quad \frac{-3\beta\|\mu\|}{2} \quad \frac{\|\mu\|}{2} \quad \frac{-7\beta\|\mu\|}{2} \quad \frac{-3\beta\|\mu\|}{2} \quad \frac{\|\mu\|}{2} \quad \frac{\|\mu\|}{2} \quad \frac{-3\beta\|\mu\|}{2} \right] & \text{for } i, j \in C_1 \times C_{-1}, \\
& \left[\frac{-3\beta\|\mu\|}{2} \quad \frac{-3\beta\|\mu\|}{2} \quad \frac{-7\beta\|\mu\|}{2} \quad \frac{\|\mu\|}{2} \quad \frac{\|\mu\|}{2} \quad \frac{-3\beta\|\mu\|}{2} \quad \frac{-3\beta\|\mu\|}{2} \quad \frac{\|\mu\|}{2} \right] & \text{for } i, j \in C_{-1} \times C_1, \\
& \left[\frac{-\beta\|\mu\|}{2} \quad \frac{-5\beta\|\mu\|}{2} \quad \frac{-5\beta\|\mu\|}{2} \quad \frac{-\beta\|\mu\|}{2} \quad \frac{\|\mu\|}{2} \quad \frac{-\|\mu\|}{2} \quad \frac{-3\beta\|\mu\|}{2} \quad \frac{-\|\beta\mu\|}{2} \right] & \text{for } i, j \in C_0 \times C_1, \\
& \left[\frac{-5\beta\|\mu\|}{2} \quad \frac{-\beta\|\mu\|}{2} \quad \frac{-\beta\|\mu\|}{2} \quad \frac{-5\beta\|\mu\|}{2} \quad \frac{-3\beta\|\mu\|}{2} \quad \frac{-\beta\|\mu\|}{2} \quad \frac{\|\mu\|}{2} \quad \frac{-\beta\|\mu\|}{2} \right] & \text{for } i, j \in C_0 \times C_{-1}, \\
& \left[\frac{-\beta\|\mu\|}{2} \quad \frac{-5\beta\|\mu\|}{2} \quad \frac{-\beta\|\mu\|}{2} \quad \frac{-5\beta\|\mu\|}{2} \quad \frac{-\beta\|\mu\|}{2} \quad \frac{\|\mu\|}{2} \quad \frac{-\beta\|\mu\|}{2} \quad \frac{-3\beta\|\mu\|}{2} \right] & \text{for } i, j \in C_1 \times C_0, \\
& \left[\frac{-5\beta\|\mu\|}{2} \quad \frac{-\beta\|\mu\|}{2} \quad \frac{-5\beta\|\mu\|}{2} \quad \frac{-\beta\|\mu\|}{2} \quad \frac{-\beta\|\mu\|}{2} \quad \frac{-3\beta\|\mu\|}{2} \quad \frac{-\|\beta\mu\|}{2} \quad \frac{\|\mu\|}{2} \right] & \text{for } i, j \in C_{-1} \times C_0, \\
& \left[\frac{-3\beta\|\mu\|}{2} \quad \frac{-3\beta\|\mu\|}{2} \quad \frac{-3\beta\|\mu\|}{2} \quad \frac{-3\beta\|\mu\|}{2} \quad \frac{-\beta\|\mu\|}{2} \quad \frac{-\beta\|\mu\|}{2} \quad \frac{-\beta\|\mu\|}{2} \quad \frac{-\beta\|\mu\|}{2} \right] & \text{for } i, j \in C_0^2.
\end{aligned}$$

Then,

$$\mathbf{r}^T \cdot \text{LeakyRelu}(\Delta_{ij}) = \begin{cases} 10R\beta\|\mu\|(1 \pm o(1)) & \text{if } i, j \in C_1^2 \\ -2R\|\mu\|(1 + 2\beta)(1 \pm o(1)) & \text{if } i, j \in C_{-1}^2 \\ -2R\|\mu\|(1 + 5\beta)(1 \pm o(1)) & \text{if } i \in C_1, j \in C_{-1} \\ 10R\beta\|\mu\|(1 \pm o(1)) & \text{if } i \in C_{-1}, j \in C_1 \\ -\frac{R}{2}\|\mu\|(1 - 21\beta)(1 \pm o(1)) & \text{if } i \in C_0, j \in C_1 \\ -\frac{R}{2}\|\mu\|(1 - 11\beta)(1 \pm o(1)) & \text{if } i \in C_0, j \in C_{-1} \\ -\frac{R}{2}\|\mu\|(1 - 5\beta)(1 \pm o(1)) & \text{if } i \in C_1, j \in C_0 \\ -\frac{R}{2}\|\mu\|(1 - 5\beta)(1 \pm o(1)) & \text{if } i \in C_{-1}, j \in C_0 \\ 2R\beta\|\mu\|(1 \pm o(1)) & \text{if } i, j \in C_0^2 \end{cases},$$

and the proof is complete. \square

Next we will define our high probability event.

Definition 2. $\mathcal{E}' \stackrel{\text{def}}{=} \mathcal{E} \cap \mathcal{E}^*$, where \mathcal{E}^* is the event that for a fixed $\mathbf{w} \in \mathbb{R}^d$, all $i \in [n]$ satisfy $|\mathbf{w}^T \mathbf{X}_i - \mathbf{E}[\mathbf{w}^T \mathbf{X}_i]| \leq 10\sigma \|\mathbf{w}\|_2 \sqrt{\log n}$.

The following lemma is obtained by using [Lemma 4](#) with standard Gaussian concentration and a union bound.

Lemma 7. With probability at least $1 - 1/\text{poly}(n)$ event \mathcal{E}' holds.

Corollary 8. Suppose that p, q satisfy [Assumption 1](#), $\|\boldsymbol{\mu}\| = \omega(\sigma\sqrt{\log n})$ and fix $R \in \mathbb{R}$. Then, there exists a choice of attention architecture Ψ such that with probability $1 - o_n(1)$ over $(\mathbf{A}, \mathbf{X}) \sim \text{CSBM}(n, p, q, \boldsymbol{\mu}, \sigma^2)$ it holds that

$$\gamma_{ij} = \begin{cases} \frac{3}{np}(1 \pm o(1)) & \text{if } i, j \in C_0^2 \cup C_1^2 \\ \frac{3}{nq}(1 \pm o(1)) & \text{if } i, j \in C_{-1} \times C_1 \\ \frac{3}{nq} \exp(-\Theta(R\|\boldsymbol{\mu}\|)) & \text{if } i, j \in C_{-1} \times C_{-1} \cup C_0 \\ \frac{3}{np} \exp(-\Theta(R\|\boldsymbol{\mu}\|)) & \text{otherwise} \end{cases},$$

where R is a parameter of the architecture.

Proof. The proof is immediate. First applying the ansatz from [Lemma 5](#) with $\beta < 1/25$, [Lemma 7](#) and a union bound. Using the definition of γ_{ij} concludes the proof. \square

Next, we prove [Thm. 1](#) that the model distinguish nodes from C_0 for any choice of p, q satisfying [Assumption 1](#). We restate the theorem for convince.

Theorem 9 (Formal restatement of [Thm. 1](#)). Suppose that p, q satisfy [Assumption 1](#) and $\|\boldsymbol{\mu}\|_2 = \omega(\sigma\sqrt{\log n})$. Then, there exists a choice of attention architecture Ψ such that with probability at least $1 - o_n(1)$ over the data $(\mathbf{X}, \mathbf{A}) \sim \text{CSBM}(n, p, q, \boldsymbol{\mu}, \sigma^2)$, the estimator

$$\hat{x}_i \stackrel{\text{def}}{=} \sum_{j \in N_i} \gamma_{ij} \tilde{\mathbf{w}}^T \mathbf{X}_j + b \quad \text{where } \tilde{\mathbf{w}} = \boldsymbol{\mu} / \|\boldsymbol{\mu}\|, \quad b = -\|\boldsymbol{\mu}\|/2$$

satisfies $\hat{x}_i < 0$ if and only if $i \in C_0$.

Proof. Let Ψ be the architecture from [Cor. 8](#) and let R satisfy $R\|\boldsymbol{\mu}\|_2 = \omega(1)$. We will compute the mean and variance of the estimator \hat{x}_i conditioned on \mathcal{E}' . Suppose that $i \in C_0$. By using [Cor. 8](#), [Definition 2](#) and our assumption on $\|\boldsymbol{\mu}\|$ and R , we have

$$\max \left\{ \frac{3}{np} \exp(-\Theta(R\|\boldsymbol{\mu}\|)), \frac{3}{nq} \exp(-\Theta(R\|\boldsymbol{\mu}\|)) \right\} = o\left(\frac{1}{n(p+2q)}\right),$$

and therefore

$$\begin{aligned} \mathbf{E}[\hat{x}_i \mid \mathcal{E}'] &= \mathbf{E} \left[\sum_{k \in \{-1, 0, 1\}} \sum_{j \in N_i \cap C_k} \gamma_{ij} \tilde{\mathbf{w}}^T \mathbf{X}_j \mid \mathcal{E}' \right] - \frac{\|\boldsymbol{\mu}\|}{2} \\ &= \mathbf{E}[|C_0 \cap N_i| \mid \mathcal{E}'] \left(\pm \frac{3}{np} (1 \pm o(1)) \cdot 10\sigma\sqrt{\log n} \right) \\ &\quad + \mathbf{E}[|C_1 \cap N_i| \mid \mathcal{E}'] \left(o\left(\frac{1}{n(p+2q)}\right) \cdot (\|\boldsymbol{\mu}\| \pm 10\sigma\sqrt{\log n}) \right) \\ &\quad + \mathbf{E}[|C_{-1} \cap N_i| \mid \mathcal{E}'] \left(o\left(\frac{1}{n(p+2q)}\right) \cdot (-\|\boldsymbol{\mu}\| \pm 10\sigma\sqrt{\log n}) \right) - \frac{\|\boldsymbol{\mu}\|}{2} \\ &= -\frac{\|\boldsymbol{\mu}\|}{2} (1 \pm o(1)). \end{aligned}$$

By similar reasoning we have that for $i \in C_{-1} \cup C_1$, $\mathbf{E}[\hat{x}_i \mid \mathcal{E}'] = \frac{\|\boldsymbol{\mu}\|}{2} (1 \pm o(1))$.

Next, we claim that for each $i \in [n]$ the random variable \hat{x}_i given \mathcal{E}' is sub-Gaussian with a small sub-Gaussian constant compared to the above expectation. The following lemma is a straightforward adaptation of [Lemma A.11](#) in [Fountoulakis et al. \(2022\)](#), and we provide its proof for completeness.

Lemma 10. Conditioned on \mathcal{E}' , the random variables $\{\hat{x}_i\}_i$ are sub-Gaussian with parameter $\tilde{\sigma}_i^2 = O\left(\frac{\sigma^2}{np}\right)$ if $i \in C_0 \cup C_1$ and $\tilde{\sigma}_i^2 = O\left(\frac{\sigma^2}{nq}\right)$ otherwise.

Proof. Fix $i \in [n]$, and write $\mathbf{X}_i = \varepsilon_i \boldsymbol{\mu} + \sigma \mathbf{g}_i$ where $\mathbf{g}_i \sim \mathcal{N}(0, \mathbf{I}_d)$, and ε_i denotes the class membership. Consider \hat{x}_i as a function of $\mathbf{g} = [\mathbf{g}_1 \circ \mathbf{g}_2 \circ \dots \circ \mathbf{g}_n] \in \mathbb{R}^{nd}$, where \circ denotes vertical concatenation. Namely, consider the function

$$\hat{x}_i = f_i(\mathbf{g}) \stackrel{\text{def}}{=} \sum_{j \in N_i} \gamma_{ij}(\mathbf{g}) \tilde{\mathbf{w}}^T (\varepsilon_j \boldsymbol{\mu} + \sigma \mathbf{g}_j) - \|\boldsymbol{\mu}\|/2, \quad i \in [n].$$

Since $\mathbf{g} \sim \mathcal{N}(0, \mathbf{I}_{nd})$, proving that \hat{x}_i given \mathcal{E}' is sub-Gaussian for each $i \in [n]$, reduces to showing that the function $f_i : \mathbb{R}^{nd} \rightarrow \mathbb{R}$ is Lipschitz over $E \subseteq \mathbb{R}^{nd}$ defined by \mathcal{E}' and the relation $\mathbf{X}_i = \varepsilon_i \boldsymbol{\mu} + \sigma \mathbf{g}_i$. That is, $E \stackrel{\text{def}}{=} \{\mathbf{g} \in \mathbb{R}^{nd} \mid |\tilde{\mathbf{w}}^T \mathbf{g}_i| \leq 10\sqrt{\log n}, \forall i \in [n]\}$. Specifically, we show that conditioning on the event \mathcal{E}' (which restricts $\mathbf{g} \in E$), the Lipschitz constant L_{f_i} of f_i satisfies $L_{f_i} = O\left(\frac{\sigma}{\sqrt{np}}\right)$ for $i \in C_0 \cup C_1$ and $L_{f_i} = O\left(\frac{\sigma}{nq}\right)$ otherwise, and hence proving the claim.

First note that event \mathcal{E}' induce a transformation which transforms isotropic Gaussians to truncated Gaussians vectors. Similarly to [Fountoulakis et al. \(2022\)](#), we can show that this transformation can be obtained by a push-forward mapping whose Lipschitz constant is 1.

$$\bar{\mathbf{v}} = M(\mathbf{v}) \stackrel{\text{def}}{=} [\tau(\mathbf{v}_1), \tau(\mathbf{v}_2), \dots, \tau(\mathbf{v}_n)]^T \quad (8)$$

where $\tau(x) \stackrel{\text{def}}{=} \Phi^{-1}((1-2c)\Phi(x) + c)$ for $c = \Phi(-10\sqrt{\log n})$.

To compute the Lipschitz constant of $f_i(\mathbf{g})$ for $i \in [n]$, let us denote $\mathbf{X} = [\mathbf{X}_1 \circ \mathbf{X}_2 \circ \dots \circ \mathbf{X}_n]$ and consider the function

$$\tilde{f}_i(\mathbf{X}) \stackrel{\text{def}}{=} \sum_{j \in N_i} \gamma_{ij}(\mathbf{X}) \tilde{\mathbf{w}}^T \mathbf{X}_j, \quad i \in [n]$$

Let us assume without loss of generality that $i \in C_0$ (the cases for $i \in C_1$ and $i \in C_{-1}$ are obtained identically). Conditioning on the event \mathcal{E}' , which imposes the restriction that $\mathbf{X} \in \tilde{E}$ where

$$\tilde{E} \stackrel{\text{def}}{=} \left\{ \mathbf{X} \in \mathbb{R}^{nd} \mid |\mathbf{X}_i - \varepsilon_i \boldsymbol{\mu}| \leq 10\sigma\sqrt{\log n}, \forall i \in [n] \right\}.$$

Conditioning on \mathcal{E}' (which restricts $\mathbf{X}, \mathbf{X}' \in \tilde{E}$), using [Cor. 8](#) and recalling that R satisfies $R\|\boldsymbol{\mu}\|_2 = \omega(1)$, we get⁴

$$\begin{aligned} & \left| \tilde{f}_i(\mathbf{X}) - \tilde{f}_i(\mathbf{X}') \right| \\ & \simeq \left| \sum_{j \in N_i \cap C_0} \frac{3}{np} \tilde{\mathbf{w}}^T (\mathbf{X}_j - \mathbf{X}'_j) + \sum_{j \in N_i \cap C_1} \frac{3}{np} \cdot e^{-\Theta(R\|\boldsymbol{\mu}\|_2)} \tilde{\mathbf{w}}^T (\mathbf{X}_j - \mathbf{X}'_j) + \sum_{j \in N_i \cap C_{-1}} \frac{3}{np} \cdot e^{-\Theta(R\|\boldsymbol{\mu}\|_2)} \tilde{\mathbf{w}}^T (\mathbf{X}_j - \mathbf{X}'_j) \right| \\ & = \left| \begin{bmatrix} \frac{3}{np} (1 \pm o(1)) \tilde{\mathbf{w}} & \text{if } j \in N_i \cap C_0 \\ \frac{3}{np} \exp(-\Theta(R\|\boldsymbol{\mu}\|_2)) (1 \pm o(1)) \tilde{\mathbf{w}} & \text{if } j \in N_i \cap C_1 \\ \frac{3}{np} \exp(-\Theta(R\|\boldsymbol{\mu}\|_2)) (1 \pm o(1)) \tilde{\mathbf{w}} & \text{if } j \in N_i \cap C_{-1} \\ 0 & \text{if } j \notin N_i \end{bmatrix}_{j \in [n]}^T (\mathbf{X} - \mathbf{X}') \right| \\ & \leq \left\| \begin{bmatrix} \frac{3}{np} (1 \pm o(1)) \tilde{\mathbf{w}} & \text{if } j \in N_i \cap C_0 \\ \frac{3}{np} \exp(-\Theta(R\|\boldsymbol{\mu}\|_2)) (1 \pm o(1)) \tilde{\mathbf{w}} & \text{if } j \in N_i \cap C_1 \\ \frac{3}{np} \exp(-\Theta(R\|\boldsymbol{\mu}\|_2)) (1 \pm o(1)) \tilde{\mathbf{w}} & \text{if } j \in N_i \cap C_{-1} \\ 0 & \text{if } j \notin N_i \end{bmatrix}_{j \in [n]} \right\|_2 \|\mathbf{X} - \mathbf{X}'\|_2 \\ & \leq \sqrt{\frac{3}{np}} (1 + o(1)) \|\tilde{\mathbf{w}}\|_2 \|\mathbf{X} - \mathbf{X}'\|_2 \\ & = \sqrt{\frac{3}{np}} (1 + o(1)) \|\mathbf{X} - \mathbf{X}'\|_2. \end{aligned}$$

⁴We drop the $(1 \pm o(1))$ in the first line of the computation for compactness and use \simeq as notation.

This shows the Lipschitz constant of $\tilde{f}_i(\mathbf{X})$ over \tilde{E} satisfies $L_{\tilde{f}_i} = O\left(\frac{1}{\sqrt{np}}\right)$. On the other hand, by viewing \mathbf{X} as a function of \mathbf{g} , it is straightforward to see that the function $h(\mathbf{g}) : \mathbb{R}^{nd} \rightarrow \mathbb{R}^{nd}$ defined by $h(\mathbf{g}) \stackrel{\text{def}}{=} \mathbf{X}(\mathbf{g})$ has Lipschitz constant $L_h = \sigma$, as

$$\|h(\mathbf{g}) - h(\mathbf{g}')\|_2 = \|\varepsilon\boldsymbol{\mu} + \sigma\mathbf{g} - (\varepsilon\boldsymbol{\mu} + \sigma\mathbf{g}')\|_2 = \sigma\|\mathbf{g} - \mathbf{g}'\|_2.$$

Therefore, since $f_i(\mathbf{g}) = \tilde{f}_i(h(\mathbf{g}))$ and $\mathbf{g} \in E$ if and only if $\mathbf{X} \in \tilde{E}$, we have that, conditioning on \mathcal{E}' , the function $\hat{x}_i = f_i(\mathbf{g})$ is Lipschitz continuous with Lipschitz constant $L_{f_i} = L_{\tilde{f}_i}L_h = O\left(\frac{\sigma}{\sqrt{np}}\right)$. Since $\mathbf{g} \sim \mathcal{N}(0, \mathbf{I}_{nd})$, we know that \hat{x}_i is sub-Gaussian with sub-Gaussian constant $\tilde{\sigma}^2 = L_{f_i}^2 = O\left(\frac{\sigma^2}{np}\right)$. \square

The following lemma will be used for bounding the misclassification probability.

Lemma 11 (Rigollet & Hütter (2015)). Let x_1, \dots, x_n be sub-Gaussian random variables with the same mean and sub-Gaussian parameter $\tilde{\sigma}^2$. Then,

$$\mathbf{E} \left[\max_{i \in [n]} (x_i - \mathbf{E}[x_i]) \right] \leq \tilde{\sigma} \sqrt{2 \log n}.$$

Moreover, for any $t > 0$

$$\Pr \left[\max_{i \in [n]} (x_i - \mathbf{E}[x_i]) > t \right] \leq 2n \exp \left(-\frac{t^2}{2\tilde{\sigma}^2} \right).$$

We bound the probability of misclassification

$$\Pr \left[\max_{i \in C_0} \hat{x}_i \geq 0 \right] \leq \Pr \left[\max_{i \in C_0} \hat{x}_i > t + \mathbf{E}[\hat{x}_i] \right],$$

for $t < |\mathbf{E}[\hat{x}_i]| = \frac{\|\boldsymbol{\mu}\|_2}{2}(1 \pm o(1))$. By Lemma 10, picking $t = \Theta\left(\sigma\sqrt{\log|C_0|}\right)$ and applying Lemma 11 implies that the above probability is $1/\text{poly}(n)$.

Similarly for class $C_1 \cup C_{-1}$ we have that the misclassification probability is

$$\begin{aligned} \Pr \left[\min_{i \in C_1 \cup C_{-1}} \hat{x}_i \leq 0 \right] &= \Pr \left[-\max_{i \in C_1 \cup C_{-1}} (-\hat{x}_i) \leq 0 \right] = \Pr \left[\max_{i \in C_1 \cup C_{-1}} (-\hat{x}_i) \geq 0 \right] \\ &\leq \Pr \left[\max_{i \in C_1 \cup C_{-1}} -\hat{x}_i > t - \mathbf{E}[\hat{x}_i] \right], \end{aligned}$$

for $t < \mathbf{E}[\hat{x}_i]$. Picking $t = \Theta\left(\sigma\sqrt{\log|C_1 \cup C_{-1}|}\right)$ and applying Lemma 11 and a union bound over the misclassification probabilities of both classes conclude the proof of the corollary. \square

Combining Thm. 9 with Lemma 3, we immediately get Cor. 2 which we restate below.

Corollary 12. Suppose $p, q = \Omega(\log^2 n/n)$ and $\|\boldsymbol{\mu}\| \geq \omega\left(\sigma\sqrt{\frac{(p+2q)\log n}{n(p-q)^2}}\right)$. Then, there is a choice of attention architecture Ψ such that, with probability at least $1 - o(1)$ over the data $(\mathbf{X}, \mathbf{A}) \sim \text{CSBM}(n, p, q, \boldsymbol{\mu}, \sigma^2)$, CAT separates nodes C_0 from $C_1 \cup C_{-1}$.

B Synthetic experiments

In this section, we present the complete results for the synthetic data experiments of §6.1. First, we describe the parameterization we use for the 1-layer GCN, GAT, and CAT models; then, we verify the behavior of the normalized score function (γ_{ij}) matches that of the theory presented in Cor. 8. In particular, we visualize the average of the following three groups of gammas (Fig. 5):

- Gammas γ_{ij} included in $i, j \in C_0^2 \cup C_1^2$. Solid lines.
- Gammas γ_{ij} included in $i, j \in C_{-1} \times C_1$. Dashed lines.
- The rest of gammas. Dotted lines.

For completeness, we also include the empirical results that validate Thm. 1 and Cor. 2, which were discussed already in §6.1.

Experimental setup. We assume the following parametrization for the 1-layer GCN, GAT, and CAT:

$$\mathbf{h}'_i = \left(\sum_{j \in N_i} \gamma_{ij} \tilde{\mathbf{w}}^T \mathbf{X}_j \right) - C \cdot \|\boldsymbol{\mu}\|/2, \quad (9)$$

where N_i are the set of neighbors of node i , \mathbf{X}_j are the features of node j —obtained from the CSBM described in §4, and \mathbf{h}'_i are the logits of the prediction of node i . Note that for GCN we have $\gamma_{ij} = \frac{1}{|N_i^*|}$. Otherwise, we consider the following parameterization of the score function Ψ :

$$\gamma_{ij} = \frac{\exp(\Psi(\mathbf{h}_i, \mathbf{h}_j))}{\sum_{k \in N_i^*} \exp(\Psi(\mathbf{h}_i, \mathbf{h}_k))} \quad \text{where} \quad (10)$$

$$\Psi(\mathbf{h}_i, \mathbf{h}_j) \stackrel{\text{def}}{=} \mathbf{r}^T \cdot \text{LeakyRelu} \left(\mathbf{S} \cdot \begin{bmatrix} \tilde{\mathbf{w}}^T \mathbf{h}_i \\ \tilde{\mathbf{w}}^T \mathbf{h}_j \end{bmatrix} + \mathbf{b} \right). \quad (11)$$

For these experiments, we define the parameters $\tilde{\mathbf{w}}$, \mathbf{S} , \mathbf{b} and \mathbf{r} as in the proofs in App. A:

$$\tilde{\mathbf{w}} \stackrel{\text{def}}{=} \frac{\boldsymbol{\mu}}{\|\boldsymbol{\mu}\|}, \quad \mathbf{S} \stackrel{\text{def}}{=} \begin{bmatrix} 1 & 1 \\ -1 & -1 \\ 1 & -1 \\ -1 & 1 \\ 0 & 1 \\ 1 & 0 \\ 0 & -1 \\ -1 & 0 \end{bmatrix}, \quad \mathbf{b} \stackrel{\text{def}}{=} \begin{bmatrix} -3/2 \\ -3/2 \\ -3/2 \\ -3/2 \\ -1/2 \\ -1/2 \\ -1/2 \\ -1/2 \end{bmatrix} \cdot \|\boldsymbol{\mu}\| \cdot C, \quad \mathbf{r} \stackrel{\text{def}}{=} R \cdot \begin{bmatrix} 2 \\ -2 \\ -2 \\ 2 \\ -1 \\ -1 \\ -1 \\ -1 \end{bmatrix}, \quad (12)$$

where $R > 0$ and $C > 0$ are arbitrary scaling parameters. Both C and R and input to the score function are set different for each of the models, as indicated in Table 4. In particular, we set $R = \frac{7}{\|\boldsymbol{\mu}\|}$ for both GAT and CAT such that: i) all γ_{ij} are distinguishable as we decrease $\|\boldsymbol{\mu}\|$; and ii) we avoid numerical instabilities in the implementation when computing the exponential of $R \times \|\boldsymbol{\mu}\|$ in order to obtain γ_{ij} (see Cor. 8), as the exponential of small or large values leads to under/overflow issues. As for C , we set $C = 1$ for GAT and $C = (p - q)/(p + 2q)$ for CAT such that we counteract the fact that the distance between classes shrink as we increase q , see Lemma 3:

Table 4: Parameters for the synthetic experiments.

Model	C	R	\mathbf{h}_i
GCN	0	—	—
GAT	1	$\frac{7}{\ \boldsymbol{\mu}\ }$	\mathbf{X}_i
CAT	$\frac{p-q}{p+2q}$	$\frac{7}{\ \boldsymbol{\mu}\ }$	$\frac{1}{ N_i^* } \sum_{k \in N_i^*} \mathbf{X}_k$

Regarding the data model, we set (as described in §6.1) $n = 10000$, $p = 0.5$, $\sigma = 0.1$, and $d = n / (5 \log^2(n))$. We set the slope of the LeakyReLU activation to $\beta = 1/5$ for the GAT and $\beta = 0.01$ for CAT, such that the proof of Cor. 8 is valid. As described in the main paper, to assess the sensitivity to structural noise, we present the complete results

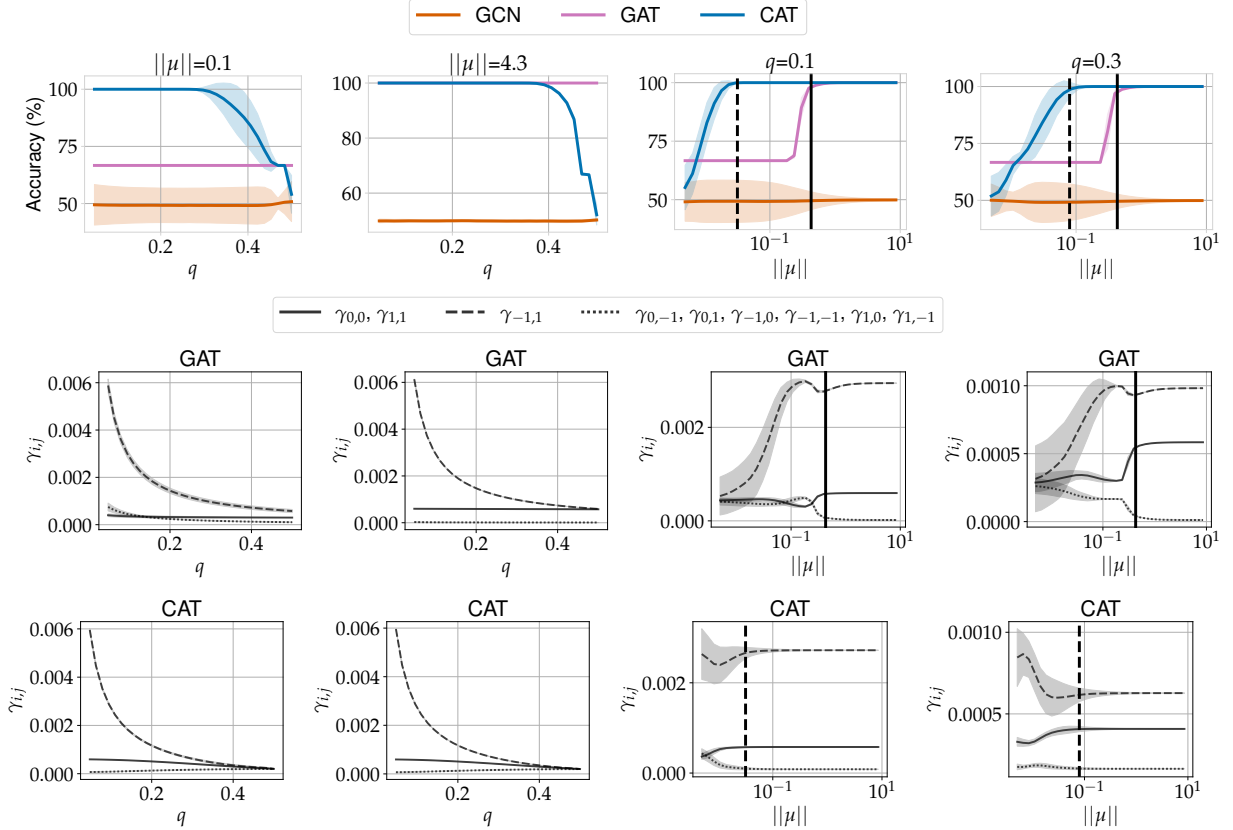


Figure 5: Synthetic data results. On the top row, we show the node classification, and in the following two rows we show the γ_{ij} values for GAT and CAT respectively. In the two left-most figures, we show how the results vary with the noise level q for $\|\mu\| = 0.1$ and $\|\mu\| = 4.3$. In the two right-most figures, we show how the results vary with the norm of the means $\|\mu\|$ for $q = 0.1$ and $q = 0.3$. We use two vertical lines to present the classification threshold stated in [Thm. 1](#) (solid line) and [Cor. 2](#) (dashed line).

for two sets of experiments. First, we vary the noise level q between 0 and 0.5, fixing the mean vector μ . We test two values of $\|\mu\|$: the first corresponds to the *easy* regime ($\|\mu\| = 10\sigma\sqrt{2\log n} \approx 4.3$) where classes are far apart; and the second correspond to the *hard* regime ($\|\mu\| = \sigma = 0.1$) where the distance between the clusters is small. In the second experiment we modify instead the distance between the means, sweeping $\|\mu\|$ in the range $[\sigma/20, 20\sigma\sqrt{2\log n}]$ which corresponds to $[0.005, 8.58]$, and thus covering the transition from the hard setting (small $\|\mu\|$) to the easy one (large $\|\mu\|$). In these experiments, we fix q to 0.1 (low noise) and 0.3 (high noise).

Results are summarized in [Fig. 5](#). The top row contains the node classification performance for each of the models (i.e., [Fig. 1](#)), the next two rows contain the γ_{ij} values for GAT and CAT respectively. The two left-most columns of [Fig. 5](#) show the results for the hard and easy regimes, respectively, as we vary the noise level q . In the hard regime, we observe that GAT is unable to achieve separation for any value of q , whereas CAT achieves perfect classification when q is small enough. The gamma plots help shed some light on this question. For GAT, we observe that the gammas represented with the dotted and solid lines collapse for any value of q (see middle plot), while this does not happen for CAT when the noise level is low (see bottom plot). This exemplifies the advantage of CAT over GAT as stated in [Cor. 2](#). When the distance between the means is large enough, we see that GAT achieves perfect results independently of q , as stated in [Thm. 1](#). We also observe that, in this case, the gammas represented with the dotted and solid lines do not collapse for any value of q . In contrast, as we increase q , CAT fails to satisfy the condition in [Cor. 2](#), and therefore achieves inferior performance. We note that the low performance is due to the fact that all gammas collapse to the same value for large noise levels.

For the second set of experiments (two right-most columns of [Fig. 1](#)), where we fix q and sweep $\|\mu\|$, we observe that, for both values of q , there exists a transition in the accuracy of both GAT and CAT as a function of $\|\mu\|$. As shown in the main manuscript, GAT achieves perfect accuracy when the distance between the means satisfies the condition in

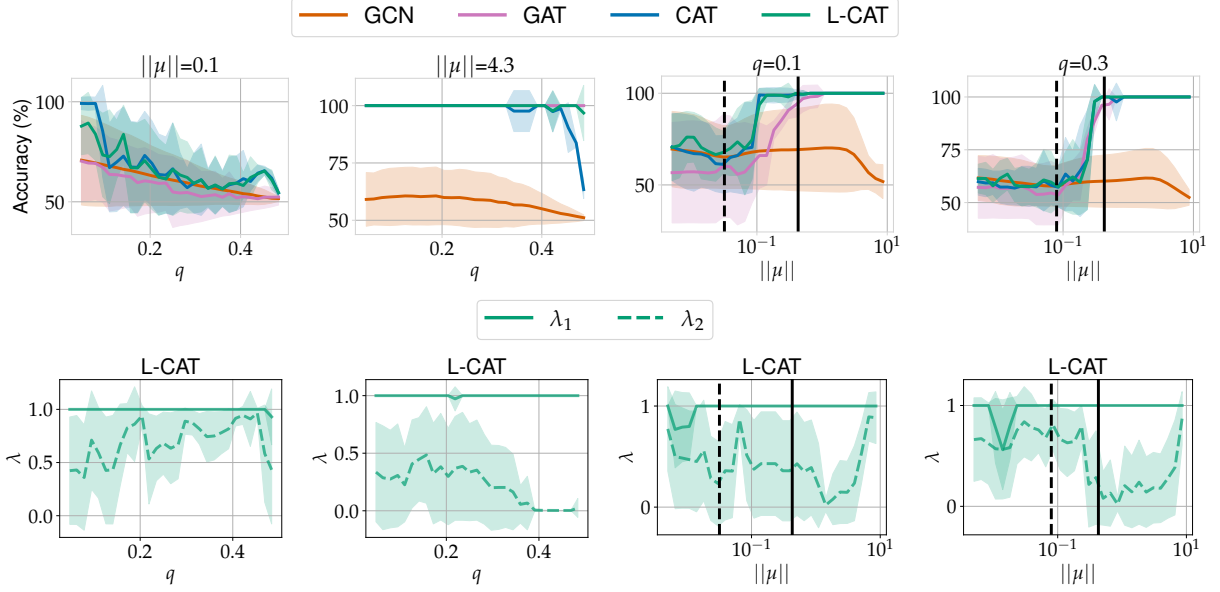


Figure 6: Synthetic data results learning C , λ_1 and λ_2 . On the top row, we show the node classification accuracy, and in the bottom row we show the learned values of λ_1 and λ_2 for L-CAT. In the two left-most figures, we show how the results vary with the noise level q for $\|\mu\| = 0.1$ and $\|\mu\| = 4.3$. In the two right-most figures, we show how the results vary with the norm of the means $\|\mu\|$ for $q = 0.1$ and $q = 0.3$. We use two vertical lines to present the classification threshold stated in [Thm. 1](#) (solid line) and [Cor. 2](#) (dashed line).

[Thm. 1](#) (solid vertical line in [Fig. 1](#)). Moreover, we can see the improvement CAT obtains over GAT. Indeed, when $\|\mu\|$ satisfies the conditions of [Cor. 2](#) (dashed vertical line in [Fig. 1](#)), the classification threshold is improved. As we increase q , we see that the gap between the two vertical lines decreases, which means that the improvement decreases as q increments, exactly as stated in [Cor. 2](#). This transition from the hard regime to the easy regime is also observed in the gamma plots: we observe the largest difference in value between the different groups of lambdas for values of $\|\mu\|$ that satisfy the condition in [Thm. 1](#) (that is to the right of the vertical lines).

B.1 Other experiments

In the following, we extend the results for the synthetic data presented above. In particular, we aim to evaluate if L-CAT is able to achieve top performance regardless of the scenario. That is, we want to evaluate if L-CAT consistently performs at least as good as the best-performing model. We change the fixed-parameter setting of the previous section and, instead, we evaluate the performance of GCN, GAT, CAT and L-CAT when we learn the model-dependent parameters.

Experimental setup. We assume the same parametrization for the 1-layer GCN, GAT and CAT described in [Eq. 9](#) and [Eq. 11](#). For L-CAT, we add the parameters λ_1 and λ_2 , as indicated in [Eq. 7](#). We fix the parameters shared among the models, that is, \tilde{w} , S , b , r , and R , with the values indicated in [Eq. 12](#). Different from previous experiments, we now learn C and, for L-CAT, we also learn λ_1 and λ_2 . We choose to fix part of the parameters (instead of learning them all) to keep the problem as similar as possible to the theoretical analysis we provided in [§4](#) and [App. A](#). If we instead learn all the parameters, it takes a single dimension of the features to be (close to) linearly separable to find a solution that achieves a similar performance regardless of the model, which hinders the analysis. This is a consequence of the probabilistic nature of the features. One way of solving this issue would be to make n big enough. Instead, we opt to have a fixed n and reduce the degrees of freedom of the models by fixing the parameters shared across all models. The rest of the experimental setup matches the one from [App. B](#). Additionally, we use the Adam optimizer ([Kingma & Ba, 2015](#)) with a learning rate of 0.05, and we train for 100.

Results are summarized in [Fig. 6](#). The top row contains the node classification performance for every model, while the bottom row contains the learned values of λ_1 (solid line) and λ_2 (dashed line) with L-CAT. The two left-most columns of [Fig. 6](#) show the results for the hard and easy regimes, respectively, as we vary the noise level q . In the hard regime, we see rather noisy results. Still, the behaviour is similar to that of [Fig. 5](#): the performance of CAT degrades as we increase q . We also observe that, on average, CAT outperforms GAT. In this case, we observe that L-CAT achieves

similar performance as CAT, which can be explained by inspecting the learned values of lambda in the bottom row. We observe that $\lambda_1 = 1$ and $\lambda_2 \geq 0.5$ on average for all values of q . This indicates that L-CAT is closer to CAT than to GAT. When the distance between the means is large enough (i.e., $\|\mu\| = 4.3$), we see that GAT achieves perfect results independently of q while the performance of CAT deteriorates with large values of q , the same trend as in Fig. 5. Remarkably, we observe that L-CAT also achieves perfect results independently of q . If we inspect the lambda values, we first see that $\lambda = 1$ for all q , thus the interpolation happens between CAT and GAT. Looking at the values of λ_2 , we observe that, for small values of q , λ_2 is pretty noisy, which is expected since any solution achieves perfect performance. Interestingly, we have that $\lambda_2 = 0$ for large values of q , with negligible variance. This indicates that L-CAT learns that it must behave like GAT in order to perform well.

For the second set of experiments (two right-most columns of Fig. 6), we fix q and sweep $\|\mu\|$ like we did in Fig. 5. Here, we observe a similar trend: for both values of q , there exists a transition in the accuracy of both GAT and CAT as a function of $\|\mu\|$. Yet once again, we observe that L-CAT consistently achieves a similar performance to the best-performing model in every situation.

C Dataset description

We present further details about the datasets used in our experiments, summarized in Table 5. All datasets are undirected (or transformed to undirected otherwise) and transductive.

The upper rows of the table refer to datasets used in §6.2 taken from the PyTorch Geometric framework.⁵ The following paragraphs present a short description of such datasets.

Amazon Computers & Photos are datasets taken from Shchur et al. (2018), in which nodes represent products, and edges indicate that the products are usually bought together. The node features are a Bag of Words (BoW) representation of the product reviews. The task is to predict the category of the products.

GitHub is a dataset introduced in Rozemberczki et al. (2021), in which nodes correspond to developers, and edges indicate mutual follow relationship. Node features are embeddings extracted from the developer’s starred repositories and profile information (e.g., location or employer). The task is to infer whether a node relates to web or machine learning development.

FacebookPagePage is a dataset introduced in Rozemberczki et al. (2021), where nodes are Facebook pages, and edges imply mutual likes between the pages. Nodes features are text embeddings extracted from the pages’ description. The task consist on identifying the page’s category.

TwitchEN is a dataset introduced in Rozemberczki et al. (2021). Here, nodes correspond to Twitch gamers, and links reveal mutual friendship. Node features are an embedding of games liked, location, and streaming habits. The task is to infer if a gamer uses explicit content.

Coauthor Physics & CS are datasets introduced in Shchur et al. (2018). In this case, nodes represent authors which are connected with an edge if they have co-authored a paper. Node features are BoW representations of the keywords of the author’s papers. The task consist on mapping each author to their corresponding field of study.

DBLP is a dataset introduced in Bojchevski & Günnemann (2018) that represents a citation network. In this dataset, nodes represent papers and edges correspond to citations. Node features are BoW representations of the keywords of the papers. The task is to predict the research area of the papers.

PubMed, Cora & CiteSeer are citation networks introduced in Yang et al. (2016). Nodes represent documents, and edges refer to citations between the documents. Node features are BoW representations of the documents. The task is to infer the topic of the documents.

The bottom rows of Table 5 refer to the datasets from Open Graph Benchmark (OGB) (Hu et al., 2020a)⁶ used in §6.3. We include a short description of them in the paragraphs below.

ogbn-arxiv is a citation network of computer science papers in arXiv (Wang et al., 2020). Nodes represent papers, and directed edges refer to citations among them. Node features are embeddings of the title and abstract of the papers. The task is to predict the research area of the nodes.

ogbn-products contains a co-purchasing network (Bhatia et al., 2016). Nodes represent products, and links are present whenever two products are bought together. Node features are embeddings of a BoW representation of the product description. The task is to infer the category of the products.

⁵<https://pytorch-geometric.readthedocs.io/en/latest/modules/datasets.html>

⁶<https://ogb.stanford.edu/docs/nodeprop>

ogbn-mag is a heterogeneous network formed from a subgraph of the Microsoft Academic Graph (MAG) (Wang et al., 2020). Nodes can belong to one of these four types: authors, papers, institutions and fields of study. Moreover, directed edges belong to one of the following categories: “author is affiliated with an institution,” “author has written a paper,” “paper cites a paper,” and “paper belongs to a research area.” Only nodes that are papers contain node features, which are a text embedding of the document content. The task is to predict the venue of the nodes that are papers.

ogbn-proteins is a network whose nodes represent proteins and edges indicate different types of associations among them. This dataset does not contain node features. The tasks are to predict multiple protein functions, each of them being a binary classification problem.

Table 5: Dataset statistics. On the top part of the table, we show the datasets used in §6.2. On the bottom part of the table, we show the datasets used in §6.3.

Name	#Nodes	#Edges	Avg. degree	#Node feats.	#Edge feats.	#Tasks	Task Type
AmazonComp.	13,752	491,722	35.76	767	-	1	10-class clf.
AmazonPhoto	7,650	238,162	31.13	745	-	1	8-class clf.
GitHub	37,700	578,006	15.33	128	-	1	Binary clf.
FacebookP.	22,470	342,004	15.22	128	-	1	4-class clf.
CoauthorPh.	34,493	495,924	14.38	8415	-	1	5-class clf.
TwitchEN	7,126	77,774	10.91	128	-	1	Binary clf.
CoauthorCS	18,333	163,788	8.93	6805	-	1	15-class clf.
DBLP	17,716	105,734	5.97	1639	-	1	4-class clf.
PubMed	19,717	88,648	4.50	500	-	1	3-class clf.
Cora	2,708	10,556	3.90	1433	-	1	7-class clf.
CiteSeer	3,327	9,104	2.74	3703	-	1	6-class clf.
ogbn-arxiv	169,343	1,166,243	6.89	128	-	1	40-class clf.
ogbn-products	2,449,029	123,718,280	50.52	100	-	1	47-class clf.
ogbn-mag	1,939,743	21,111,007	18.61	128	4	1	349-class clf.
ogbn-proteins	132,534	79,122,504	597.00	-	8	112	Multi-task

D Real data experiments

D.1 Experimental details

Computational resources. We used CPU cores to run this set of experiments. In particular, for each trial, we used 2 CPU cores and up to 16 GB of memory. We ran the experiments in parallel using a shared cluster with 10000 CPU cores approximately.

General experimental setup. As mentioned in §6.2, we repeat all experiments 10 times, which correspond to 10 different random initialization of the parameters of the GNNs. In all cases, we choose the model parameters with the best validation performance during training. In order to run the experiments and collect the results, we used the GraphGym framework (You et al., 2020), which includes the data processing and loading of the datasets, as well as the evaluation and collection of the results. We split the datasets in 70 % training, 15 % validation, and 15 % test.

We cross-validate the number of message-passing layers in the network (2, 3, 4), as well as the learning rate ([0.01, 0.005]). Then, we report the results of the best validation error among the 4 possible combinations. However, in practice we found the best performance always to use 4 message-passing layers, and thus the only difference in configuration lies in the learning rate.

We use residual connections between the GNN layers, 4 heads in the attention models, and the Parametric ReLU (PReLU) (He et al., 2015) as the nonlinear activation function. We do not use batch normalization (Ioffe & Szegedy, 2015), nor dropout (Srivastava et al., 2014). We use the Adam optimizer (Kingma & Ba, 2015) with $\beta = (0.9, 0.999)$, and an exponential learning-rate scheduler with $\gamma = 0.998$. We train all the models for 2500 epochs. Importantly, we do not use weight decay, since this will bias the solution towards $\lambda_1 = 0$ and $\lambda_2 = 1$.

We use the Pytorch Geometric (Fey & Lenssen, 2019) implementation of L-CAT for all experiments, switching between models by properly by setting λ_1 and λ_2 . We parametrize λ_1 and λ_2 as free-parameters in log-space that pass through a sigmoid function—i.e., $\text{sigmoid}(10^x)$ —such that they are constrained to the unit interval, and they are learned quickly.

D.2 Additional results

Table 6 shows the results presented in the main paper (with the addition of a dense feed-forward network), while Table 7 presents the results for the remaining datasets, with smaller average degree.

If we focus on Table 7, we observe that all models perform equally well, yet in a few cases CAT and L-CAT are significantly better than the baselines—e.g., L-CATv2 in *CoauthorCS*, or L-CAT in *Cora*. Following a similar discussion as the one presented in the main paper, these results indicates that L-CAT achieves similar or better performance than baseline models and thus, should be the preferred architecture.

Competitive performance without the graph. We also include in Tables 6 and 7 the performance of a feed-forward network, referred to as Dense (first row). Note that the only data available to this model are the node features, and thus no graph information is provided. Therefore, we should expect a significant drop in performance, which indeed happens for some datasets such as *Amazon Computers* ($\approx 7\%$ drop), *FacebookPagePage* ($\approx 20\%$ drop), *DBLP* ($\approx 9\%$ drop) and *Cora* ($\approx 14\%$ drop). Still, we found that for other commonly used datasets the performance is similar, e.g., *Coauthor Physics* and *PubMed*; or it is even better *CoauthorCS*. These results manifest the importance of a proper benchmarking, and of carefully considering the datasets used to evaluate GNN models.

Table 6: Test accuracy (%) of the considered convolution and attention models for different datasets (sorted by their average node degree), and averaged over ten runs. Bold numbers are statistically different to their baseline model ($\alpha = 0.05$). Best average performance is underlined.

Dataset	<i>Amazon Computers</i>	<i>Amazon Photo</i>	<i>GitHub</i>	<i>Facebook PagePage</i>	<i>Coauthor Physics</i>	<i>TwitchEN</i>
Avg. Deg.	35.76	31.13	15.33	15.22	14.38	10.91
Dense	83.73 \pm 0.34	91.74 \pm 0.46	81.21 \pm 0.30	75.89 \pm 0.66	95.41 \pm 0.14	56.26 \pm 1.74
GCN	<u>90.59 \pm 0.36</u>	<u>95.13 \pm 0.57</u>	84.13 \pm 0.44	94.76 \pm 0.19	96.36 \pm 0.10	57.83 \pm 1.13
GAT	89.59 \pm 0.61	94.02 \pm 0.66	83.31 \pm 0.18	94.16 \pm 0.48	96.36 \pm 0.10	57.59 \pm 1.20
CAT	90.58 \pm 0.40	94.77 \pm 0.47	84.11 \pm 0.66	94.71 \pm 0.30	<u>96.40 \pm 0.10</u>	<u>58.09 \pm 1.61</u>
L-CAT	90.34 \pm 0.47	94.93 \pm 0.37	84.05 \pm 0.70	<u>94.81 \pm 0.25</u>	<u>96.35 \pm 0.10</u>	<u>57.88 \pm 2.07</u>
GATv2	89.49 \pm 0.53	93.47 \pm 0.62	82.92 \pm 0.45	93.44 \pm 0.30	96.24 \pm 0.19	57.70 \pm 1.17
CATv2	90.44 \pm 0.46	94.81 \pm 0.55	84.10 \pm 0.88	94.27 \pm 0.31	96.34 \pm 0.12	57.99 \pm 2.02
L-CATv2	90.33 \pm 0.44	94.79 \pm 0.61	<u>84.31 \pm 0.59</u>	94.44 \pm 0.39	96.29 \pm 0.13	57.89 \pm 1.53

Table 7: Test accuracy (%) of the considered convolution and attention models for different datasets (sorted by their average node degree), and averaged over ten runs. Bold numbers are statistically different to their baseline model ($\alpha = 0.05$). Best average performance is underlined.

Dataset	<i>CoauthorCS</i>	<i>DBLP</i>	<i>PubMed</i>	<i>Cora</i>	<i>CiteSeer</i>
Avg. Deg.	8.93	5.97	4.5	3.9	2.74
Dense	<u>94.88 \pm 0.21</u>	75.46 \pm 0.27	88.13 \pm 0.33	72.75 \pm 1.72	73.02 \pm 1.01
GCN	93.85 \pm 0.23	84.18 \pm 0.40	88.50 \pm 0.18	<u>86.68 \pm 0.78</u>	<u>75.76 \pm 1.09</u>
GAT	93.80 \pm 0.38	84.15 \pm 0.39	<u>88.62 \pm 0.18</u>	85.95 \pm 0.95	75.40 \pm 1.43
CAT	93.70 \pm 0.31	84.10 \pm 0.29	<u>88.58 \pm 0.25</u>	85.85 \pm 0.79	75.64 \pm 0.91
L-CAT	93.65 \pm 0.23	84.13 \pm 0.26	88.45 \pm 0.32	86.66 \pm 0.87	75.04 \pm 1.12
GATv2	93.19 \pm 0.64	84.33 \pm 0.18	88.52 \pm 0.27	85.65 \pm 1.01	75.14 \pm 1.20
CATv2	93.51 \pm 0.34	84.15 \pm 0.41	88.54 \pm 0.29	85.50 \pm 0.94	74.68 \pm 1.30
L-CATv2	93.65 \pm 0.20	84.31 \pm 0.31	88.48 \pm 0.24	85.75 \pm 0.72	75.04 \pm 1.30

E Open Graph Benchmark experiments

E.1 Experimental details

Computational resources. For this set of experiments, we had at our disposal a set of 16 Tesla V100-SXM GPUs with 160 CPU cores, shared among the rest of the department.

Statistical significance. For each CAT and L-CAT model, we highlight significant improvements according to a two-sided paired t-test ($\alpha = 0.05$), with respect to its corresponding baseline model. For example, for L-CATv2 with 8 heads we perform the test with respect to GATv2 with 8 heads.

General experimental setup. As mentioned in §6.3, we repeat all experiments with OGB datasets 5 times. In all cases, we choose the model parameters with the best validation performance during training. Moreover, when we show the results without specifying the number of heads, we take the model with the best validation error among the two models with 1 and 8 heads.

We use the same implementation of L-CAT for all experiments, switching between models by properly setting λ_1 and λ_2 . Experiments on *arxiv*, *mag*, *products* use a version of L-CAT implemented in Pytorch Geometric (Fey & Lenssen, 2019). Experiments on *proteins* use a version of L-CAT implemented in DGL (Wang et al., 2019a). We parametrize λ_1 and λ_2 as free-parameters in log-space that pass through a sigmoid function—i.e., $\text{sigmoid}(10^x)$ —such that they are constrained to the unit interval, and they are learned quickly.

ArXiv. As described in §6.3, we use the example code from the OGB framework (Hu et al., 2020a). The network is composed of 3 GNN layers with a hidden size of 128. We use batch normalization (Ioffe & Szegedy, 2015) and a dropout (Srivastava et al., 2014) of 0.5 between the GNN layers, and Adam (Kingma & Ba, 2015) with a learning rate of 0.01. We use the ReLU as activation function. For the initial experiments, we train for 1500 epochs, while we train for 500 epochs for the noise experiments in §6.3.1. This is justified given the convergence plots in Fig. 2.

MAG. We adapted the official code from (Brody et al., 2022). The network is composed of 2 layers with 128 hidden channels. This time, we use layer normalization (Ba et al., 2016) and a dropout of 0.5 between the layers. Again, we use ReLU as the activation function, and add residual connections to the network. As with *arxiv*, we use Adam (Kingma & Ba, 2015) with learning rate 0.01. We set a batch size of 20000 and train for 100 epochs.

Products. We use the same setup as (Brody et al., 2022), with a network of 3 GNN layers and 128 hidden dimensions. We apply residual connections once again, with a dropout (Srivastava et al., 2014) of 0.5 between layers. This time, we use ELU as the activation function. The batch size is set to 256. Adam (Kingma & Ba, 2015) is again the optimizer in use, this time with a learning rate of 0.001. We train for 100 epochs, although we apply early stopping whenever the validation accuracy stops increasing for more than 10 epochs. Note the training split of this dataset only contains 8% of the data.

Proteins. We follow once more the setup of (Brody et al., 2022). The network we use has 6 GNN layers of hidden size 64. Dropout (Srivastava et al., 2014) is set to 0.25 between layers, with an input dropout of 0.1. At the beginning of the network, we place a linear layer followed by a ReLU activation to encode the nodes, and a linear layer at the end of the network to predict the class. Moreover, we use batch normalization (Ioffe & Szegedy, 2015) between layers and ReLU as the activation function. We train the model for 1200 epochs at most, with early stopping after not improving for 10 epochs.

E.2 Additional results

We show in Tables 8 to 10 the results of the main paper for the *arxiv*, *mag*, *products* datasets, respectively, without selecting the best configuration for each type of model. That is, we show the results for both number of heads. Note that we already show the full table of results for the *protein* datasets in the main paper (Table 3). All the trends discussed in the main paper hold.

Table 8: Test accuracy on the *arxiv* dataset for attention models using 1 head and 8 heads.

	GCN	GAT	CAT	L-CAT	GATv2	CATv2	L-CATv2
1h	71.58 ± 0.19	71.58 ± 0.15	72.04 ± 0.20	72.00 ± 0.11	71.70 ± 0.14	72.02 ± 0.08	71.96 ± 0.21
8h	—	71.63 ± 0.11	72.14 ± 0.20	71.98 ± 0.08	71.72 ± 0.24	71.76 ± 0.14	71.91 ± 0.16

Extrapolation ablation study. Due to page constraints, these results were not added to the main paper. Here, we study two questions. First, how important are λ_1 and λ_2 in the formulation of L-CAT (Eq. 7)? For the sake of completeness, the second question we attempt to answer here is whether we can obtain similar performance by just interpolating

Table 9: Test accuracy on the *mag* dataset for attention models using 1 head and 8 heads.

	GCN	GAT	CAT	L-CAT	GATv2	CATv2	L-CATv2
1h	<u>32.77 ± 0.36</u>	32.35 ± 0.24	31.98 ± 0.46	32.47 ± 0.38	32.76 ± 0.18	32.43 ± 0.22	32.68 ± 0.50
8h	–	32.15 ± 0.31	31.58 ± 0.22	32.49 ± 0.21	<u>32.85 ± 0.21</u>	32.34 ± 0.18	32.38 ± 0.28

Table 10: Test accuracy on the *products* dataset for attention models using 1 head and 8 heads.

	GCN	GAT	CAT	L-CAT	GATv2	CATv2	L-CATv2
1h	74.12 ± 1.20	<u>78.53 ± 0.91</u>	77.38 ± 0.36	77.19 ± 1.11	73.81 ± 0.39	74.81 ± 1.12	76.37 ± 0.92
8h	–	<u>78.23 ± 0.25</u>	76.63 ± 1.15	76.56 ± 0.45	76.40 ± 0.71	75.20 ± 0.92	74.70 ± 0.28

between GCN and GAT (fixing $\lambda_2 = 0$)? Note that we theoretically showed in §§4 and 6.1 that CAT fills up a gap between GCN and GAT, making it preferable in certain settings.

To this end, we repeat the experiments for network-initialization robustness in §6.3.2, since they showed to be the best ones to tell apart the performance across models. We include three additional models: GCN-GAT, which interpolates between GCN and GAT (or GATv2) by learning λ_1 and fixing $\lambda_2 = 0$; CAT- λ_1 which interpolates between GCN and CAT by learning λ_1 and fixing $\lambda_2 = 1$; and CAT- λ_2 , which interpolates between GAT and CAT by learning λ_2 and fixing $\lambda_1 = 1$.

Results using GAT and shown in Table 11, and using GATv2 in Table 12. We can observe that GCN-GAT obtains results in between GCN and GAT for all settings, despite being able to interpolate between both layers in each of the six layers of the network. Regarding learning λ_1 and λ_2 , we can observe that there is a clear difference between learning both (L-CAT), and learning a single one. For both attention models, CAT- λ_1 obtains better results than CAT- λ_2 in all settings, but *uniform* with 8 heads. Still, the results of both variants are substantially worse than those of L-CAT in all cases, *demonstrating the importance of learning to interpolate between the three layer types*.

Table 11: Test accuracy on the *proteins* dataset for GCN (Kipf & Welling, 2017) and GAT (Velickovic et al., 2018) attention models using two network initializations, and two numbers of heads (1 and 8).

	GCN	GCN-GAT	GAT	CAT	L-CAT	CAT- λ_1	CAT- λ_2
<i>uniform</i> initialization							
1h	61.08 ± 2.86	70.44 ± 1.56	59.73 ± 4.04	74.19 ± 0.72	<u>77.77 ± 1.44</u>	71.97 ± 3.78	73.55 ± 1.36
8h	–	68.51 ± 0.91	72.23 ± 3.20	73.60 ± 1.27	<u>78.85 ± 1.76</u>	76.43 ± 2.47	72.76 ± 2.79
<i>normal</i> initialization							
1h	<u>80.10 ± 0.61</u>	66.51 ± 3.23	66.38 ± 7.76	73.26 ± 1.84	78.06 ± 1.40	76.77 ± 1.91	73.39 ± 1.25
8h	–	69.93 ± 1.93	79.08 ± 1.64	74.67 ± 1.29	<u>79.63 ± 0.79</u>	78.86 ± 1.07	73.32 ± 1.15

Table 12: Test accuracy on the *proteins* dataset for GCN (Kipf & Welling, 2017) and GATv2 (Brody et al., 2022) attention models using two network initializations, and two numbers of heads (1 and 8).

	GCN	GCN-GATv2	GATv2	CATv2	L-CATv2	CATv2- λ_1	CATv2- λ_2
<i>uniform</i> initialization							
1h	61.08 ± 2.86	69.69 ± 1.59	59.85 ± 3.05	64.32 ± 2.61	<u>79.08 ± 1.06</u>	63.24 ± 1.55	73.41 ± 0.34
8h	–	69.94 ± 1.62	75.21 ± 1.80	74.16 ± 1.45	<u>78.77 ± 1.09</u>	77.61 ± 1.32	73.96 ± 1.27
<i>normal</i> initialization							
1h	<u>80.10 ± 0.61</u>	68.54 ± 1.63	69.13 ± 9.48	74.33 ± 1.06	79.07 ± 1.09	78.41 ± 0.93	74.07 ± 1.17
8h	–	68.71 ± 1.96	78.65 ± 1.61	73.40 ± 0.62	<u>79.30 ± 0.55</u>	78.76 ± 1.41	73.22 ± 0.77

F Extending L-CAT to other GNN models

Due to their simplicity and popularity, in the manuscript we focus on the simplest form of GCNs, as described in §2. However, we consider important to remark that L-CAT can be effortlessly extended to a large range of existing GNN models. A more general formulation of a message-passing GNN layer than the one given in Eq. 1 is the following:

$$\tilde{\mathbf{h}}_i = f(\mathbf{h}'_i) \quad \text{where} \quad \mathbf{h}'_i \stackrel{\text{def}}{=} \bigoplus_{j \in N_i^*} \hat{\gamma}_{ij} M(\mathbf{h}_i, \mathbf{h}_j; \theta_M), \quad (13)$$

where $\hat{\gamma}_{ij}$ is a scalar value, \bigoplus refers to any permutation invariant operation—e.g., sum, mean, maximum, or minimum operations—and M is the message operator, which can be parameterized, and produces a message based on the sender and receiver representations. This formulation comprises most GNN architectures present in the current literature. For example:

- GCN (Kipf & Welling, 2017): $\mathbf{h}'_i = \sum_{j \in N_i^*} \hat{\gamma}_{ij} \mathbf{W}_v \mathbf{h}_j$ where $\hat{\gamma}_{ij} = \frac{1}{|N_i^*|}$ as consider in the main paper, or $\hat{\gamma}_{ij} = \frac{1}{\sqrt{d_j d_i}}$, where d_i is the number of neighbors of node i (including self-loops), if we consider the symmetric normalized adjacency matrix instead.
- GIN (Xu et al., 2019): $\mathbf{h}'_i = (1 + \varepsilon) \hat{\gamma}_{ii} \mathbf{h}_i + \sum_{j \in N_i^*} \hat{\gamma}_{ij} \mathbf{h}_j$ with $\hat{\gamma}_{ij} = 1$.
- PNA (Corso et al., 2020): $\mathbf{h}'_i = \bigoplus_{j \in N_i^*} \hat{\gamma}_{ij} M(\mathbf{h}_i, \mathbf{h}_j; \theta_M)$ where $\hat{\gamma}_{ij} = 1$, M is an multi-layer perceptron, and \bigoplus is a set of permutation invariant operations, e.g., $\bigoplus = [\mu, \sigma, \max, \min]$.
- GCNII (Chen et al., 2020): $\mathbf{h}'_i = \left(\alpha \mathbf{h}_i^0 + (1 - \alpha) \sum_{j \in N_i^*} \hat{\gamma}_{ij} \mathbf{h}_j \right) \left((1 - \beta) \mathbf{I} + \beta \mathbf{W}_v \right)$ where, just as in the GCN case, $\hat{\gamma}_{ij} = \frac{1}{\sqrt{d_j d_i}}$, and $0 \leq \alpha, \beta \leq 1$.

In all the models above, the values $\hat{\gamma}_{ij}$ are taken from the adjacency matrix A (whose entries are 1 if there exists an edge between nodes i and j , and 0 otherwise), or a matrix derived from it, e.g., the symmetric normalized adjacency matrix.

Note that the attention coefficients γ_{ij} defined in Eq. 3 can be understood as an attention-equivalent of the adjacency matrix. Indeed, by defining A^{att} as a matrix whose entries are $|N_i^*| \gamma_{ij}$, one can obtain a row-stochastic matrix that can substitute the adjacency matrix of any GNN model. This technique to generalize attention models to GNN variants more complex than a GCN has been successfully applied in prior literature (Wang et al., 2021b).

With this new interpretation of attention-models, the interpolation performed by L-CAT (see Eq. 7) can similarly be re-interpreted. Indeed, L-CAT learns to interpolate between the adjacency matrix A , and an attention-based adjacency matrix A^{att} , which can be produced by either GAT (Eq. 3) or CAT (Eq. 6), depending on the value of λ_2 .

F.1 PNA experiments

In Tables 13 and 14, we show the results—for the datasets described in App. C—using L-CAT and CAT in conjunction with the PNA model (Corso et al., 2020). First, we note that standard PNA works quite well in most cases. Second, if we focus on Table 13, we observe that the standard attention models (i.e., PNAGAT and PNAGATv2) perform significantly worse than the other approaches, in particular on datasets with large average degree, e.g., on *Amazon Computers*. Finally, we observe that the L-CAT models (i.e., L-PNACAT and L-PNACATv2) drastically improve the performance of their attention counterparts and achieve similar performance as the PNA model, with lower performance on the *GitHub* and *Facebook* datasets and higher performance on *Cora* and *CiteSeer*.

To keep the same number of parameters, we reuse the PNA weights to compute the attention scores ($\mathbf{W}_q = \mathbf{W}_k = \mathbf{W}_v$). However, this could be detrimental, as the role of \mathbf{W}_v is completely different from that of \mathbf{W}_q and \mathbf{W}_k . Tables 15 and 16 show the same experiments as before, but using different parameters to compute the keys and queries (i.e., $\mathbf{W}_q = \mathbf{W}_k \neq \mathbf{W}_v$). We observe that the increase of parameters generally helps both CAT and L-CAT models, now outperform the base PNA model in some settings.

Table 13: Test accuracy (%) of the PNA (Corso et al., 2020) models for different datasets (sorted by average node degree), averaged over ten runs. Bold numbers are statistically different to their baseline model ($\alpha = 0.05$). Best average performance is underlined.

Dataset	<i>Amazon Computers</i>	<i>Amazon Photo</i>	<i>GitHub</i>	<i>Facebook PagePage</i>	<i>Coauthor Physics</i>	<i>TwitchEN</i>
Avg. Deg.	35.76	31.13	15.33	15.22	14.38	10.91
PNA	<u>86.51 ± 1.22</u>	<u>93.23 ± 0.65</u>	<u>82.33 ± 0.51</u>	<u>94.28 ± 0.34</u>	96.09 ± 0.14	<u>59.25 ± 1.19</u>
PNAGAT	57.59 ± 10.19	74.78 ± 8.74	72.77 ± 2.06	71.49 ± 11.23	96.05 ± 0.25	54.22 ± 3.02
PNACAT	81.48 ± 3.81	91.73 ± 1.24	75.55 ± 3.33	93.10 ± 0.41	96.16 ± 0.15	59.11 ± 1.94
L-PNACAT	86.45 ± 1.42	92.76 ± 0.74	78.74 ± 2.91	93.59 ± 0.39	<u>96.24 ± 0.13</u>	59.12 ± 2.74
PNAGATv2	36.93 ± 4.07	60.13 ± 4.81	73.93 ± 1.89	58.91 ± 3.42	95.61 ± 0.29	54.45 ± 1.60
PNACATv2	79.08 ± 2.62	88.61 ± 3.24	75.11 ± 2.79	92.77 ± 0.50	96.06 ± 0.18	56.72 ± 2.43
L-PNACATv2	85.10 ± 1.70	92.19 ± 0.55	79.79 ± 1.40	93.54 ± 0.36	96.03 ± 0.19	58.19 ± 1.53

Table 14: Test accuracy (%) of the PNA (Corso et al., 2020) models for different datasets (sorted by average node degree), averaged over ten runs. Bold numbers are statistically different to their baseline model ($\alpha = 0.05$). Best average performance is underlined.

Dataset	<i>CoauthorCS</i>	<i>DBLP</i>	<i>PubMed</i>	<i>Cora</i>	<i>CiteSeer</i>
Avg. Deg.	8.93	5.97	4.5	3.9	2.74
PNA	<u>93.30 ± 0.31</u>	83.37 ± 0.32	88.37 ± 0.73	84.94 ± 1.19	73.92 ± 0.97
PNAGAT	92.46 ± 0.95	83.42 ± 0.39	<u>88.40 ± 0.33</u>	84.67 ± 0.69	74.64 ± 0.82
PNACAT	92.90 ± 0.24	83.35 ± 0.40	<u>88.24 ± 0.30</u>	85.58 ± 1.00	74.94 ± 1.68
L-PNACAT	93.11 ± 0.24	83.21 ± 0.55	88.22 ± 0.40	85.77 ± 1.01	<u>75.08 ± 1.05</u>
PNAGATv2	90.14 ± 0.82	83.37 ± 0.34	88.14 ± 0.45	85.04 ± 0.86	74.50 ± 1.18
PNACATv2	92.78 ± 0.27	83.22 ± 0.38	88.28 ± 0.30	85.41 ± 0.98	74.42 ± 1.11
L-PNACATv2	93.02 ± 0.37	<u>83.54 ± 0.65</u>	88.23 ± 0.58	85.48 ± 0.98	74.76 ± 1.57

Table 15: Test accuracy (%) of the PNA (Corso et al., 2020) extended models with $W_q = W_k \neq W_v$ for different datasets, averaged over ten runs. Bold numbers are statistically different to their baseline model ($\alpha = 0.05$). Best average performance is underlined.

Dataset	<i>Amazon Computers</i>	<i>Amazon Photo</i>	<i>GitHub</i>	<i>Facebook PagePage</i>	<i>Coauthor Physics</i>	<i>TwitchEN</i>
Avg. Deg.	35.76	31.13	15.33	15.22	14.38	10.91
PNA	<u>86.51 ± 1.22</u>	<u>93.23 ± 0.65</u>	<u>82.33 ± 0.51</u>	<u>94.28 ± 0.34</u>	96.09 ± 0.14	<u>59.25 ± 1.19</u>
PNAGAT	48.65 ± 19.25	68.01 ± 20.32	72.97 ± 1.07	70.17 ± 12.02	96.02 ± 0.34	53.27 ± 2.54
PNACAT	83.45 ± 2.60	91.62 ± 1.30	75.35 ± 2.71	93.31 ± 0.55	96.22 ± 0.13	59.23 ± 2.25
L-PNACAT	87.18 ± 1.22	92.79 ± 0.63	79.64 ± 2.54	93.78 ± 0.39	96.31 ± 0.17	59.09 ± 2.50
PNAGATv2	39.49 ± 4.09	62.19 ± 11.30	73.97 ± 1.67	63.00 ± 4.95	95.83 ± 0.36	55.21 ± 1.05
PNACATv2	81.20 ± 3.63	91.32 ± 0.80	74.57 ± 2.18	92.98 ± 0.36	96.14 ± 0.16	56.21 ± 2.01
L-PNACATv2	86.22 ± 0.83	92.98 ± 0.89	79.78 ± 2.48	93.44 ± 0.37	96.13 ± 0.12	60.26 ± 1.25

F.2 GCNII experiments

Similarly, we have run the experiments from §6.2, this time combining GCNII (Chen et al., 2020) with GAT, CAT, and L-CAT as explained above. Results are shown in Tables 17 and 18, in which we can observe that the baseline model obtains the best results so far in the manuscript (in comparison with both GCN and PNA). And just as before, we observe again that CAT and L-CAT always improve with respect to their base models, staying on par with the baseline GCNII model and, sometimes, even outperforming the baseline model on average (e.g., *Coauthor Physics*, *TwitchEN*). As with the experiments for PNA, Tables 19 and 20 shows the results when the attention matrices are different from the

Table 16: Test accuracy (%) of the PNA (Corso et al., 2020) extended models with $W_q = W_k \neq W_v$ for different datasets, averaged over ten runs. Bold numbers are statistically different to their baseline model ($\alpha = 0.05$). Best average performance is underlined.

Dataset	<i>CoauthorCS</i>	<i>DBLP</i>	<i>PubMed</i>	<i>Cora</i>	<i>CiteSeer</i>
Avg. Deg.	8.93	5.97	4.5	3.9	2.74
PNA	<u>93.30 ± 0.31</u>	83.37 ± 0.32	88.37 ± 0.73	84.94 ± 1.19	73.92 ± 0.97
PNAGAT	92.50 ± 0.46	83.22 ± 0.45	88.43 ± 0.29	84.89 ± 1.15	75.76 ± 1.29
PNAGAT	92.97 ± 0.47	83.28 ± 0.59	88.27 ± 0.43	85.09 ± 0.70	75.44 ± 1.51
PNAGAT	93.17 ± 0.30	83.50 ± 0.29	88.54 ± 0.45	85.63 ± 0.92	75.22 ± 1.12
PNAGATv2	90.00 ± 1.01	83.40 ± 0.48	88.14 ± 0.31	85.16 ± 0.91	76.14 ± 1.33
PNAGATv2	92.74 ± 0.20	83.05 ± 0.49	88.38 ± 0.31	85.21 ± 0.83	75.80 ± 1.26
PNAGATv2	93.02 ± 0.30	83.24 ± 0.44	88.28 ± 0.35	85.04 ± 0.94	75.80 ± 1.19

Table 17: Test accuracy (%) of the GCNII (Chen et al., 2020) models for different datasets, averaged over ten runs. Bold numbers are statistically different to their baseline model ($\alpha = 0.05$). Best average performance is underlined.

Dataset	<i>Amazon Computers</i>	<i>Amazon Photo</i>	<i>GitHub</i>	<i>Facebook PagePage</i>	<i>Coauthor Physics</i>	<i>TwitchEN</i>
Avg. Deg.	35.76	31.13	15.33	15.22	14.38	10.91
GCNII	<u>90.82 ± 0.20</u>	<u>95.51 ± 0.48</u>	<u>84.11 ± 0.76</u>	<u>94.03 ± 0.30</u>	96.58 ± 0.11	60.94 ± 1.66
GCNIIGAT	89.04 ± 0.87	94.74 ± 0.57	82.34 ± 0.64	91.18 ± 0.82	96.69 ± 0.13	57.76 ± 1.76
GCNIICAT	89.83 ± 0.42	95.31 ± 0.25	83.15 ± 0.51	93.25 ± 0.37	96.69 ± 0.09	60.51 ± 1.12
L-GCNIICAT	90.03 ± 0.42	95.23 ± 0.39	83.50 ± 0.57	93.71 ± 0.33	96.87 ± 0.14	61.14 ± 1.64
GCNIIGATv2	84.26 ± 2.80	89.23 ± 5.30	81.23 ± 0.45	83.82 ± 1.24	96.14 ± 0.28	56.25 ± 1.56
GCNIICATv2	89.59 ± 0.45	95.03 ± 0.55	82.45 ± 0.30	92.55 ± 0.52	96.50 ± 0.09	59.04 ± 1.49
L-GCNIICATv2	89.81 ± 0.48	95.24 ± 0.35	83.05 ± 0.49	93.68 ± 0.35	96.75 ± 0.11	61.10 ± 1.11

value matrix ($W_q = W_k \neq W_v$). We can similarly observe that most of the results are improved with the additional parameters, beating the baseline model in different datasets.

Table 18: Test accuracy (%) of the GCNII (Chen et al., 2020) models for different datasets, averaged over ten runs. Bold numbers are statistically different to their baseline model ($\alpha = 0.05$). Best average performance is underlined.

Dataset	<i>CoauthorCS</i>	<i>DBLP</i>	<i>PubMed</i>	<i>Cora</i>	<i>CiteSeer</i>
Avg. Deg.	8.93	5.97	4.5	3.9	2.74
GCNII	<u>95.36 ± 0.18</u>	83.86 ± 0.14	89.05 ± 0.28	<u>86.49 ± 0.79</u>	76.46 ± 0.71
GCNIIGAT	95.32 ± 0.27	83.45 ± 0.60	88.24 ± 0.34	85.72 ± 1.05	75.78 ± 0.77
GCNIICAT	95.12 ± 0.25	83.86 ± 0.23	88.65 ± 0.40	85.51 ± 0.95	76.60 ± 0.50
L-GCNIICAT	95.30 ± 0.29	83.76 ± 0.26	88.72 ± 0.35	85.48 ± 0.96	76.76 ± 0.51
GCNIIGATv2	93.37 ± 0.73	83.70 ± 0.42	88.49 ± 0.34	85.82 ± 1.35	75.98 ± 0.71
GCNIICATv2	95.01 ± 0.32	83.93 ± 0.36	88.60 ± 0.27	85.72 ± 1.03	76.62 ± 0.63
L-GCNIICATv2	95.29 ± 0.23	<u>83.93 ± 0.41</u>	89.12 ± 0.35	85.73 ± 0.88	76.22 ± 0.98

Table 19: Test accuracy (%) of the GCNII (Chen et al., 2020) extended models with $W_q = W_k \neq W_v$ for different datasets, averaged over ten runs. Bold numbers are statistically different to their baseline model ($\alpha = 0.05$). Best average performance is underlined.

Dataset	<i>Amazon Computers</i>	<i>Amazon Photo</i>	<i>GitHub</i>	<i>Facebook PagePage</i>	<i>Coauthor Physics</i>	<i>TwitchEN</i>
Avg. Deg.	35.76	31.13	15.33	15.22	14.38	10.91
GCNII	<u>90.82 ± 0.20</u>	95.51 ± 0.48	<u>84.11 ± 0.76</u>	<u>94.03 ± 0.30</u>	96.58 ± 0.11	<u>60.94 ± 1.66</u>
GCNIIGAT	89.24 ± 0.59	94.66 ± 0.59	82.45 ± 0.65	90.90 ± 0.71	<u>96.90 ± 0.16</u>	58.12 ± 2.02
GCNIICAT	89.94 ± 0.40	95.03 ± 0.37	83.12 ± 0.37	93.39 ± 0.31	96.59 ± 0.07	59.60 ± 0.76
L-GCNIICAT	90.35 ± 0.46	95.53 ± 0.35	83.48 ± 0.47	93.63 ± 0.39	96.80 ± 0.09	60.77 ± 2.15
GCNIIGATv2	85.70 ± 2.58	91.24 ± 2.43	81.43 ± 0.39	84.59 ± 0.79	96.55 ± 0.20	55.23 ± 2.15
GCNIICATv2	89.56 ± 0.67	95.46 ± 0.54	82.50 ± 0.47	93.04 ± 0.40	96.55 ± 0.10	59.57 ± 1.45
L-GCNIICATv2	90.24 ± 0.32	95.53 ± 0.28	83.34 ± 0.45	93.67 ± 0.47	96.73 ± 0.14	60.65 ± 1.13

Table 20: Test accuracy (%) of the GCNII (Chen et al., 2020) extended models with $W_q = W_k \neq W_v$ for different datasets, averaged over ten runs. Bold numbers are statistically different to their baseline model ($\alpha = 0.05$). Best average performance is underlined.

Dataset	<i>CoauthorCS</i>	<i>DBLP</i>	<i>PubMed</i>	<i>Cora</i>	<i>CiteSeer</i>
Avg. Deg.	8.93	5.97	4.5	3.9	2.74
GCNII	95.36 ± 0.18	83.86 ± 0.14	<u>89.05 ± 0.28</u>	<u>86.49 ± 0.79</u>	76.46 ± 0.71
GCNIIGAT	95.36 ± 0.20	83.60 ± 0.32	88.33 ± 0.35	85.26 ± 1.19	76.30 ± 0.78
GCNIICAT	95.20 ± 0.12	83.89 ± 0.29	88.45 ± 0.29	86.44 ± 1.22	76.70 ± 0.60
L-GCNIICAT	<u>95.47 ± 0.16</u>	83.70 ± 0.40	88.08 ± 0.47	86.02 ± 1.43	76.54 ± 0.59
GCNIIGATv2	93.97 ± 0.57	83.67 ± 0.24	88.24 ± 0.16	85.28 ± 1.11	76.58 ± 0.64
GCNIICATv2	95.05 ± 0.33	83.78 ± 0.35	88.35 ± 0.34	86.49 ± 0.90	75.28 ± 0.84
L-GCNIICATv2	95.45 ± 0.18	83.86 ± 0.24	88.06 ± 0.32	<u>86.49 ± 1.31</u>	<u>76.80 ± 0.42</u>